NONLINEAR CONVOLUTION FINITE ELEMENT METHOD FOR SOLUTION OF LARGE DEFORMATION ELASTODYNAMICS

A. Amiri-Hezaveh[1], M. Ostoja-Starzewski[2], and H. Moghaddasi[3]

[1]Department of Mechanical Science and Engineering, University of Illinois at Urbana-Champaign, US
[2]Department of Mechanical Science and Engineering, University of Illinois at Urbana-Champaign, US
[2] Institute for Condensed Matter Theory and Beckman Institute, University of Illinois at Urbana-Champaign, US
[3]Department of Civil and Environmental Engineering, University of Strathclyde, Glasgow, Scotland, G1 1XQ, UK

November 23, 2022

ABSTRACT

A new algorithm based on the convolution finite element method (CFEM) is proposed for the nonlinear wave propagation in elastic media. The formulation is developed in the context of the total Lagrangian framework, encompassing contributions due to both geometrical and material nonlinearities. As a basis, a counterpart of equations of motion–namely, the alternative field equations– is first established. The satisfaction of the alternative field equations is then realized in a weak sense. Next, the Newton-Raphson procedure and the consistent tangential matrix are applied to the weak formulation, where the CFEM is used as the linear solver in each iteration. Finally, several examples are carried out to examine the theoretical aspects and the feasibility of the proposed algorithm. In particular, problems of free vibration of Neo-Hookean and Saint Venant-Kirchhoff plates are explored. Also, a cantilever beam of the Neo-Hookean material is simulated for the case of forced vibrations. Conspicuously, the new solution procedure is a higher-order method in the sense that, in contrast to the existing time step methods, the accurate solution is obtained when the time-step size is increased.

***K*eywords** convolution finite element method, initial boundary value problems, nonlinear elastodynamics, conservation of energy, conservation of angular momentum

1 Introduction

It is well-understood that, in general, the Newmark family of algorithms falls short of satisfying the energy identity and conservation of angular momentum in the nonlinear elastodynamics and nonlinear dynamics of rigid bodies. In more detail, as demonstrated in [1], when there is a negligible error in the Newton Raphson method, the energy at each step varies in the following form (colored lines) [1]:

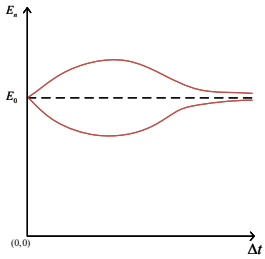

Figure 1: Failure of the average acceleration method in conserving energy of free vibration of nonlinear elastodynamics problems [1].

The algorithms addressing this non-conserving behavior belong to one of three categories [2]: 1) algorithmic damping methods 2) approaches through which conservation laws are imposed as additional restrictions to the solution procedure 3) algorithmic energy-momentum conserving approaches.

Algorithmic damping approaches have been employed to solve nonlinear problems since they cut off the contribution of higher modes by introducing controllable algorithmic damping in the linear regime. This desirable property excludes the spurious part of the solution, which may improve the stability of the method in the nonlinear analysis. However, as pointed out in [2], in such scenarios, the energy dissipation is not ensured for all parameters in the nonlinear regime.

The conservation laws are enforced as additional restrictions in the second category. The central methodology to achieve this goal is the use of the method of Lagrange multipliers. This method was introduced as an energy-conserving algorithm (i.e., the discrete form of the energy identity is satisfied) in [3]. Nevertheless, [4], based on numerical observations, concluded:" *constraint conservation of energy alone does not guarantee a stable time integration in nonlinear dynamics.*" Consequently, with the help of Langrage-multipliers, the authors of that study generalized the method by enforcing the conservation of linear and angular momentum in addition to the energy conservation. Although, as demonstrated numerically, the algorithm works suitably, the process is accompanied by high computational cost.

In the third class, often through variational integrators, the conservation of energy and momentums is achieved algorithmically. Variational integrators are a category of numerical integration used in the Hamiltonian mechanics that may conserve characteristics (constants) of the motion (see [5]). According to a statement in [6], symplectic algorithms—a category of variational integrators that conserves two-form in the phase space— with constant time step fails to exactly conserve the energy. Although for some computational purposes, the energy at each time step in the symplectic methods may be satisfactory, this is not the case in general [7]. Hence, a two-steps finite difference approach has been proposed in [7]. In the first step, by applying the midpoint rule, a symplectic integrator, exact conservation of angular and linear momentum is satisfied. On the other hand, the energy conservation is met by solving a nonlinear equation by which stress at the midpoint is written in terms of initial and end times (second step). It has been shown that the equation has an exact solution for Saint Venant-Kirchhoff materials, giving the stress of midpoint as the average values of the initial and the endpoint at each time-step.

However, it would be advantageous to develop a method that conserves constants of motion in which there is no need to solve an extra equation. With this goal in mind, [8] introduced a discrete-time derivative, proposing a similar second-order accurate approach that satisfies invariants of motion for general hyperelastic materials. The main idea behind the energy-conserving methods is defining a consistent discrete form of stress where it precisely resembles the time rate of change of potential energy. Also, as reported in [9], the technique developed initially in [7] neglects the coupling of the weak form and the above-mentioned nonlinear equations. This fact may result in divergence of the method [9]. Hence, in [9], the original algorithm has been improved by considering the coupling effect. Another progress in that vein, similar to linear elastodynamics, is developing algorithms damping out the spurious part of the solution in the nonlinear regimes. The noticeable studies in this regard can be found in the comprehensive works [10, 11], where the exclusion of high frequencies has been achieved by introducing dissipative terms in the original energy-momentum conserving algorithms in [12, 13] and [8]. It should be mentioned that, in effect, there is a family of energy-momentum conserving algorithms since the definition of the new form of stress used in this category is not unique. This fact has been shown in [14], concluding that" *there are indeed infinite ways of obtaining second order accurate, energy and momentum preserving methods.*" In addition to these studies, in [15], a combined two-step finite difference method has been unutilized for conservation of energy and momenta.

The above-mentioned methods are based on finite difference methods. On the other hand, [16] developed an energy-momentum conserving space-time FEM based on Hamiltonian's principle. In particular, the dynamical system resulting from the spatial discretization of elastodynamics problems has been written as a system of first-order ODEs, where a time finite element approach has been introduced to solve these equations. While the time finite element method

conserves energy theoretically, special attention is required for numerical implementation since the formulation involves integrals that cannot be evaluated exactly. Accordingly, they supplemented the method with a criterion fulfilling the conservation of energy. Also, for the linear shape functions, the preservation of angular momentum further imposes a stronger restriction in the choice of numerical quadrature. In continuation of [16], the authors have shown that a higher-order accuracy could be obtained through their method [17].
Overall, in most of the aforementioned studies, it has been attempted to propose new methods recovering unconditional stability and higher-order accuracy present in nonlinear problems. The use of the finite difference methods leads to define either new parameters or a new definition of stress in the discrete format. For example, in the third category, the key point is to define a new form of stress to secure satisfaction of the energy and angular momentum, leading to a new set of nonlinear equations compared to when using conventional time integration methods such as the trapezoidal method. For instance, in contrast to the Newmark method, as we shall see in the numerical section, special attention should be paid to the energy-momentum conservation methods when the denominator of the corresponding equations goes to zero. Hence, it is desirable to introduce a method that preserves the aforementioned constants while following simple steps similar to those encountered when using traditional time integration methods.

Furthermore, although the conservation of energy and angular momentum are sufficient criteria in developing a stable method, accuracy is yet another crucial factor to be considered. As mentioned in [14], the family of energy-momentum conserving methods consisting of the discrete derivative combined with the mid-point rule is at most second-order accurate. Hence, analogous to the linear problems, developing methods capable of capturing the solution when larger time steps are used is of great importance in the nonlinear regime. Accordingly, it is advantageous to enrich the literature by introducing a method containing the following attributes:

a. The form of resulting nonlinear equations is similar to those obtained by applying standard time integration methods.

b. The conservation of the invariants of motion is achievable provided that the nonlinear solver converges.

c. Higher accuracy is systematically achievable provided that the nonlinear solver converges.

d. The computational cost of the method is comparable with that of the existing methods.

In this contribution, we aim to establish a new approach that satisfies the above items. The method is based on an alternative formulation and the corresponding integral form introduced in [18]. This framework has received less attention than other methods since, at first glance, it seems to be a more complicated formulation than original equations of motion. However, in [19], by introducing the convolution finite element method (CFEM), it has been shown that this framework inherits some numerical features that cannot be found in the classical numerical methods:

1 Although it stems from space-time coupled variational form, its implementation is similar to classical time integration methods.

2 Higher accuracy for any given time interval is achievable.

3 Provided that a sufficient number of terms is considered, it uniformly converges to the exact solution in any given time interval.

4 Time-space discretization to increase the accuracy is not required.

5 Algorithm's computational cost is justifiable if compared to the classical methods.

Also, it has been demonstrated in a number of works that the framework can be developed for various types of physical processes (see [20, 21, 22, 23], among others). Recently, based on the alternative form and similar approach established in [19], a nonlinear solver has been developed for nonlinear dynamical systems in [24]. These desired characteristics motivated us to develop a dynamic nonlinear finite element scheme for nonlinear elastodynamics involving geometrical and material nonlinearities. The present study is organized as follows. First, alternative field equations pertaining to the nonlinear governing equations of motion in the material coordinate system is obtained. The satisfaction of the governing equations is assured through weak formulation in terms of convolution product. Subsequently, the Newton-Raphson method equipped with the CFEM are applied as the linear solver is employed to solve the nonlinear integral forms. As a result, in each step of the iteration, the algorithm inherits the characteristics 1-5 mentioned earlier. Next, the properties of the method are investigated in section 5. In particular, we show that the method preserves constants of motion in an adaptive manner. That is, by increasing the number of time-wise terms, the satisfaction of those identities is met regardless of the number of time steps. Finally, to show the plausibility of the method, we shall consider two examples in section 6: 1. free vibration of Neo-Hookean and Saint Venant–Kirchhoff plates to manifest how the new method conserves energy and obtains accurate solution when an adequate number of time-wise terms is assumed; 2. forced vibration of Neo-Hookean cantilever beam undergoing large deformation.

2 Problem Statement

In this study, we develop a theory based on the total Lagrangian formulation. Furthermore, material and spatial coordinate systems are shown by uppercase and lowercase letters, respectively. Also, the superscript zero is used to distinguish the reference configurations from the current one. For instance, the domain of the problem is denoted by $\mathscr{B}^0$ and $\mathscr{B}$ in the reference and current configurations, respectively. The domain $\mathscr{B}$ is assumed to be an open and Lipschitz subset of 3D Euclidean space with the boundary $\partial\mathscr{B}$. Let $\partial\mathscr{B}^0_{u_i}$ and $\partial\mathscr{B}^0_{t_i}$ denote open subsets of $\partial\mathscr{B}^0$ $(i=1,2,3)$ with $\partial\mathscr{B}^0_{u_i}\cap\partial\mathscr{B}^0_{t_i}=\emptyset$ and $\partial\mathscr{B}^0_{u_i}\cup\partial\mathscr{B}^0_{t_i}=\partial\mathscr{B}$. Also, $\overline{\mathscr{B}}$, $\overline{\partial\mathscr{B}^0_{u_i}}$, and $\overline{\partial\mathscr{B}^0_{t_i}}$ denote, respectively, closure of $\mathscr{B}$, $\partial\mathscr{B}^0_{u_i}$, and $\partial\mathscr{B}^0_{t_i}$. Then, the motion of the nonlinear hyperelastic body is governed by the following field equations and the initial and boundary conditions:

1. Equations of Motion:

$$\rho_0\ddot{u}_i(\mathbf{X},t)=P_{iJ,J}(\mathbf{X},t)+\rho_0 b_i(\mathbf{X},t),\qquad P_{iJ}F_{jJ}=P_{jJ}F_{iJ}\quad on\quad \mathscr{B}^0\times(0,T^{total}). \tag{2.1}$$

2. Kinematic Equations:

$$E_{IJ}=\frac{1}{2}(C_{IJ}-I_{IJ})=\frac{1}{2}(F_{iI}F_{iJ}-I_{IJ})=\quad on\quad \mathscr{B}^0\times(0,T^{total}). \tag{2.2}$$

3. Constitutive Equations:

$$S_{IJ}=\ 2\rho_0\frac{\partial\psi(\mathbf{C})}{\partial C_{IJ}}\quad on\ \mathscr{B}^0\times(0,T^{total}). \tag{2.3}$$

4. Boundary Conditions:

$$\begin{aligned} &u_i=\mathscr{G}_i(\mathbf{X},t) && on\quad \partial\mathscr{B}^0_{u_i}\times(0,T^{total}),\\ &P_{iJ}N_J=\mathscr{H}_i(\mathbf{X},t) && on\quad \partial\mathscr{B}^0_{t_i}\times(0,T^{total}). \end{aligned} \tag{2.4}$$

5. Initial Conditions:

$$\begin{aligned} &u_i(\mathbf{X},0)=u_i^0(\mathbf{X}) && on\quad \overline{\mathscr{B}^0},\\ &\dot{u}_i(\mathbf{X},0)=\dot{u}_i^0(\mathbf{X}) && on\quad \overline{\mathscr{B}^0}. \end{aligned} \tag{2.5}$$

in which

$$F_{iJ}=u_{iJ}(\mathbf{X},t)+\delta_{iJ},\ \mathscr{J}=\det\mathbf{F},\rho_0=\mathscr{J}\rho,P_{iJ}=\mathscr{J}\sigma_{ij}F^{-1}_{Jj},S_{IJ}=F^{-1}_{Ij}P_{jJ}, \tag{2.6}$$

where the superimpostion of material and spatial coordinate systems has been assumed; $\mathbf{P}$, $\boldsymbol{\sigma}$, ρ are nominal stress, Cauchy stress tensor, and mass density, respectively (for more details, see [25, 26]).
Next, we define the 'strong solution' of the initial boundary value problem. In doing so, we have the following regularity conditions:

Definition 1. *An ordered array* $[\mathbf{u},\mathbf{E},\mathbf{P}]$ *is called an admissible process on* $\overline{\mathscr{B}^0}\times(0,T^{total})$ *if*

$$u_i(\mathbf{X},t)\in C^{1,2},E_{IJ}(\mathbf{X},t)\in C^{0,0},P_{iJ}(\mathbf{X},t)\in C^{1,0}, \tag{2.7}$$

where smoothness of a tensor function $\mathbf{f}$ *is expressed by* $C^{M,N}$*:* $\mathbf{f}\in C^{M,N}$*, in which* $\mathbf{f}$ *is a function of position and time defined on* $\overline{\mathscr{B}^0}\times(0,T)$*, if and only if the function* $\mathbf{f}$ *and all spatial and temporal derivatives up to, respectively, orders* M *and* N *exist and are continuous.*

Definition 2. *An admissible process* $[\mathbf{u},\mathbf{E},\mathbf{P}]$ *is called a strong solution of the initial boundary value problem (IBVP) if (2.1), (2.2), (2.3), (2.4), and (2.5) hold.*

By using the Laplace transform, it can be shown that the following equations are equivalent to the equations of motion and the initial conditions:

$$\rho_0 u_i(\mathbf{X},t)=\left[t*(P_{iJ,J}+\rho_0 b_i)\right](\mathbf{X},t)+\rho_0 u_i^0(\mathbf{X})+t\rho_0\dot{u}_i^0(\mathbf{X}),\ \ P_{iJ}F_{jJ}=P_{jJ}F_{iJ}\quad on\quad \mathscr{B}^0\times(0,T^{total}), \tag{2.8}$$

in which the symbol $[h*g](\mathbf{X},t)$, for given functions $h(\mathbf{X},t)$ and $g(\mathbf{X},t)$, denotes the convolution product in the sense of

$$[f*g](\mathbf{X},t)=\int_0^t f(\mathbf{X},t-\tau)g(\mathbf{X},\tau)d\tau. \tag{2.9}$$

Also, the following notation is used in the sequel:

$$[f*g*h](\mathbf{X},t)=\int_0^t\left(\int_0^\lambda f(\mathbf{X},\lambda-\tau)g(\mathbf{X},\tau)d\tau\right)h(\mathbf{X},t-\lambda)d\lambda. \tag{2.10}$$

Hence, one can conclude:

Theorem 1. *An ordered array* $[\mathbf{u},\mathbf{E},\mathbf{P}]$ *is a strong solution of the IBVP if and only if (2.2), (2.3), (2.4) , and (2.8) hold.*

Since the alternative governing equations (2.8) consists of geometrical and materials nonlineariy, a nonlinear solver has to be employed to deal with the problem. Thus, the modified Newton-Raphson procedure is implemented. To this end, we partition the total time T^{total} into $0=T_0<T_1<...<T_{N_s}=T^{total}=N_s(1-\gamma)T$, and solve the problem consecutively, $0<\gamma<1$ is a parameter to circumvent non-convergence issue stemming from the spatial-temporal shape functions used in the sequel, and N_s denotes the number of time-steps. Now, to obtain the solution for $t=T_{pa+1},\ \ pa=0,...N_s-1$, the following terminologies are utilized:

$$\begin{aligned}&u_i^{pa}(\mathbf{X},t)=u_i^{pa}(\mathbf{X},t+T_{pa}),\ I_i^{pa}(\mathbf{X},t)=u_i(\mathbf{X},T_{pa})+t\dot{u}_i(\mathbf{X},T_{pa}),\ b_i^{Pa}(\mathbf{X},t)=b_i(\mathbf{X},t+T_{pa}),\\&\mathscr{G}_i^{pa}(\mathbf{X},t)=\mathscr{G}_i(\mathbf{X},t+T_{pa}),\ \ \mathscr{H}_i^{pa}(\mathbf{X},t)=\mathscr{H}_i(\mathbf{X},t+T_{pa}),\ 0\leqslant t\leqslant T\end{aligned} \tag{2.11}$$

where $u_i^{T_{pa}}(\mathbf{X})$ and $\dot{\mathbf{u}}^{T_{pa}}(\mathbf{X})$ denote the solutions of the previous step which are used as the initial data for the current step. It should be emphasized that the time-step Δt utilized in time integration methods is $\Delta t=(1-\gamma)T$ in the new approach. In what follows, without loss of generality, we develop the formulation to obtain the solution at $t=T_{pa+1}$.

3 Convolution Weak Formulation

The procedure of obtaining a weak solution is elaborated in this section. For completeness, we reiterate some statements from [19]:

Definition 3. *Denote* $L^2(0,T;\mathrm{H}^1(\mathscr{B}^0))$ *as a Hilbert space with inner product*

$$\int_0^T(u(t),v(t))dt, \tag{3.1}$$

whose elements are in the Hilbert space $\mathrm{H}^1(\mathscr{B}^0)$ *for* $0\leq t\leq T$ *and*

$$\int_0^T\|u(t)\|^2dt<\infty. \tag{3.2}$$

Additionally, in (3.1) and (3.2), $(,)$ *and* $\|\|$ *represent the inner product and norm of* $\mathrm{H}(\mathscr{B}^0)$*, respectively.*

Now, we have the following statement:

Lemma 1. [19] *Let* ϑ *be an element of* $L^2(0,T;\mathrm{H}^1(\mathscr{B}^0))$*, and the following holds*

$$\int_{\mathscr{B}^0}\omega(\mathbf{X})dV\int_0^T\vartheta(\mathbf{X},T-\tau)\cos(\frac{j\pi\tau}{T})d\tau=0,\quad j=0,...,\infty, \tag{3.3}$$

for every $\omega\in\mathrm{H}^1(\mathscr{B}^0)$*. Then*

$$\vartheta=0\qquad on\quad \overline{\mathscr{B}^0}\times[0,T], \tag{3.4}$$

in the sense of

$$\int_{\mathscr{B}^0}\int_0^T\vartheta^2(\mathbf{X},t)dtd\mathscr{B}=0. \tag{3.5}$$

The statement in Lemma 1 can be written in terms of all weight functions $w\in L^2(0,T;\mathrm{H}^1(\mathscr{B}^0))$:

Remark 1. [19] *Let* $\vartheta \in L^2(0,T;\mathrm{H}^1(\mathscr{B}^0))$ *such that*

$$\int_{\mathscr{B}^0} [\vartheta * w](\mathbf{X},T)d\mathscr{B} = 0, \tag{3.6}$$

for every $w \in L^2(0,T;\mathrm{H}^1(\mathscr{B}^0))$. *Then* $\vartheta = 0$ *in the sense of* (3.5).

It is worth noting that conceptually one can define a weak formulation corresponding to (2.8) where either the classical dot product or convolution product in time is utilized. However, for the case of spatial-temporal shape functions utilized in what follows, there is no difference between two products.
Next, let us define the solution and variation spaces:

Definition 4. $\mathbb{S}_i$ *and* $\mathbb{V}_i$ *stand for, respectively, the solution space and the variation space whose elements have the following properties:*

$$\mathbb{S}_i = \{u_i^{pa} \in L^2(0,T;H^1(\mathscr{B}^0)) |\ u_i^{pa}(\mathbf{X},t) = \mathscr{G}_i^{pa}(\mathbf{X},t) \ \ on \ \ \partial\mathscr{B}^0_{u_i} \times (0,T)\}, \tag{3.7}$$

$$\mathbb{V}_i = \{w_i \in L^2(0,T;H^1(\mathscr{B}^0)) | w_i = 0 \ on \ \ \partial\mathscr{B}^0_{u_i} \times (0,T)\}, \ \ i = 1,2,3. \tag{3.8}$$

Now, considering the above statements, applying the divergence theorem, one can obtain the following integral form from (2.8):

$$\begin{aligned} &\int_{\mathscr{B}^0} \rho_0 \left[u_i^{pa} * w_i\right](\mathbf{X},T)d\mathscr{B} + \int_{\mathscr{B}^0} \left[t * F_{iQ}(\mathbf{X}+\mathbf{u}^{pa}) S_{QJ}(\mathbf{X}+\mathbf{u}^{pa}) * w_{i,J}\right](\mathbf{X},T)d\mathscr{B} = \\ &\sum_{i=1}^{3} \int_{\partial\mathscr{B}^0_{t_i}} \left[t * \mathscr{H}_i^{pa} * w_i\right](\mathbf{X},T)d\Gamma + \int_{\mathscr{B}^0} \left[t * \rho_0 b_i^{pa} * w_i\right](\mathbf{X},T)d\mathscr{B} + \int_{\mathscr{B}^0} \rho_0 \left[\left(u_i^{T_{pa}} + t\dot{u}_i^{T_{pa}}\right) * w_i\right](\mathbf{X},T)d\mathscr{B}, \end{aligned} \tag{3.9}$$

in which w_i, an element of $\mathbb{V}_i$, represents weighting functions. It is noted that the convolution in time is associative, and therefore there is no need to indicate the order of time convolutions under the space integrals. In view of the Remark 1, satisfaction of (3.9) for all weight functions $w_i \in \mathbb{V}_i$ results in satisfaction of alternative governing equations in the sense of (3.5). Hence, we define:

Definition 5. $u_i(\mathbf{X},t)$, *and element of* $\mathbb{S}_i$, *is called a weak solution corresponding to the strong solution if* (3.9) *is true for all* $w_i \in \mathbb{V}_i$.

As can be seen, in contrast to classical methods, the velocity and acceleration fields are no longer present in the formulation. Moreover, initial conditions need no special attention since they are satisfied as forcing terms.

3.1 Spatial and Temporal Expansions

Now, to obtain the solution of (3.9), we employ the convolution formulation introduced in [19]. To this end, we seek the solution of (3.9) in the finite solution space (i.e., $\mathbb{S}^{h,N}$) with the corresponding finite variation space (i.e., $\mathbb{V}^{h,N}$) defined as [19]:

$$\begin{aligned} \mathbb{S}_i^{h,N} &= \mathbb{S}_i^{h,X} \otimes \mathbb{F}_N^{h,t}, \\ \mathbb{V}^{h,N} &= \mathbb{V}_i^{h,X} \otimes \mathbb{F}_N^{h,t}, \qquad (\mathbf{X},t) \in \overline{\mathscr{B}^0} \times (0,T) \end{aligned} \tag{3.10}$$

where $\mathbb{S}_i^{h,X}$ and $\mathbb{V}_i^{h,X}$ denote the following finite dimensional subsets of $\mathrm{H}^1(\mathscr{B}^0)$:

$$\begin{aligned} \mathbb{S}_i^{h,X} &= \{f(\mathbf{X}) | f(\mathbf{X}) \in \mathrm{H}^1(\mathscr{B}^0)\}, \\ \mathbb{V}_i^{h,X} &= \{g(\mathbf{X}) | g(\mathbf{X}) \in \mathrm{H}^1(\mathscr{B}^0), g(\mathbf{X}) = 0 \ \ on \ \ \partial\mathscr{B}^0_{u_i}\}, \end{aligned} \tag{3.11}$$

and

$$\mathbb{F}_N^{h,t} = \left\{1, \cos\frac{\pi t}{T}, ..., \cos\frac{(N-1)\pi t}{T}\right\}. \tag{3.12}$$

Now, to establish a Galerkin formulation, we consider the solution as:

$$u_i^{pa^h}(\mathbf{X},t) = \mathscr{V}_i^{pa^h}(\mathbf{X},t) + \overline{\mathscr{G}}_i^{pa^h}(\mathbf{X},t) + I_i^{pa}(\mathbf{X},t), \tag{3.13}$$

where

$$\begin{aligned}&\overline{\mathscr{G}}_i^{pa^h}(\mathbf{X},t)=\mathscr{G}_i^{pa}(\mathbf{X},t)-I_i^{pa}(\mathbf{X},t),\ on\quad \partial\mathscr{B}_{u_i}^0\times(0,T),\\&\overline{\mathscr{G}}_i^{pa^h}(\mathbf{X},0)=\dot{\overline{\mathscr{G}}}_i^{pa^h}(\mathbf{X},0)=0\quad on\quad \mathscr{B}^0.\end{aligned}\tag{3.14}$$

Additionally, to shorten equations, we define:

$$\mathscr{X}_i^{pa^h}(\mathbf{X},t)=X_i+\overline{\mathscr{G}}_i^{pa^h}(\mathbf{X},t)+I_i^{pa}(\mathbf{X},t)\tag{3.15}$$

Thus, the equation (3.9) can be alternatively written as:

$$\begin{aligned}&\int_{\mathscr{B}^0}\rho_0\left[\mathscr{V}_i^{pa^h}*w_i\right](\mathbf{X},T)d\mathscr{B}+\int_{\mathscr{B}^0}\rho_0\left[\overline{\mathscr{G}}_i^{pa^h}*w_i\right](\mathbf{X},T)d\mathscr{B}\\&+\int_{\mathscr{B}^0}\left[t*F_{iQ}(\boldsymbol{\mathscr{X}}^{pa^h}+\boldsymbol{\mathscr{Y}}^{pa^h})S_{QJ}(\boldsymbol{\mathscr{X}}^{pa^h}+\boldsymbol{\mathscr{Y}}^{pa^h})*w_{i,J}\right](\mathbf{X},T)d\mathscr{B}\\&-\sum_{i=1}^{3}\int_{\partial\mathscr{B}_{t_i}^0}\left[t*\mathscr{H}_i^{pa}*w_i\right](\mathbf{X},T)d\Gamma-\int_{\mathscr{B}^0}\left[t*\rho b_i^{pa}*w_i\right](\mathbf{X},T)d\mathscr{B}=0,\end{aligned}\tag{3.16}$$

with

$$\begin{aligned}&\mathscr{V}_i^{pa^h}(\mathbf{X},t)=0\ \ on\quad \partial\mathscr{B}_{u_i}^0\times(0,T),\\&\mathscr{V}_i^{pa^h}(\mathbf{X},0)=\dot{\mathscr{V}}_i^{pa^h}(\mathbf{X},0)=0\quad on\quad \mathscr{B}^0.\end{aligned}\tag{3.17}$$

To obtain the solution for (3.16), we write:

$$\boldsymbol{\mathscr{Y}}^{pa^h}(\mathbf{X},t)=\sum_{P=0}^{N-1}\sum_{j=1}^{n_{dof}}\sum_{\lambda\in\eta-\eta_{gj}}c_{Pi\lambda}\,\psi_\lambda(\mathbf{X})\cos(\frac{P\pi t}{T})\mathbf{e}_j,\tag{3.18}$$

in which $\eta=\{1,2,...,n_{np}\}$ stands for the set of all nodal points defining geometry of the problem; η_{gj} indicates the set of all nodal points on the boundary $\partial\mathscr{B}_{u_j}^0$; n_{dof} represents number of degrees of freedom which could be 1, 2, or 3; ψ_λ's show Lagrangian shape functions; $\mathbf{e}_i$, denotes unit vectors of Cartesian coordinate system in the current configuration, and $c_{Pj\lambda}$'s are unknown constant that are determined by satisfaction of (3.16). Analogous to the basis function utilized in (3.18), the test function $\mathbf{w}(\mathbf{X},t)$ is set as:

$$\mathbf{w}(\mathbf{X},t)=\sum_{Q=0}^{N-1}\sum_{i=1}^{n_{dof}}\sum_{\beta\in\eta-\eta_{gi}}d_{Qi\beta}\,\psi_\beta(\mathbf{X})\cos(\frac{Q\pi t}{T})\mathbf{e}_i,\tag{3.19}$$

where $d_{iQ\beta}$'s are arbitrary constants.

4 Newton-Raphson Procedure

To proceed, the modified Newton-Raphson procedure is implemented in this section. In doing so, we define:

$$\begin{aligned}&\boldsymbol{\mathscr{Y}}^{pa^h(m+1)}(\mathbf{x},t)=\boldsymbol{\mathscr{Y}}^{pa^h(m)}(\mathbf{x},t)+\Delta\boldsymbol{\mathscr{Y}}^{pa^h(m)}(\mathbf{x},t),\quad m=0,...,\mathscr{L}-1,\\&\boldsymbol{\mathscr{Y}}^{pa^h(0)}(\mathbf{x},t)=\mathbf{0},\end{aligned}\tag{4.1}$$

in that

$$\begin{aligned}&\boldsymbol{\mathscr{Y}}^{pa^h(m)}(\mathbf{X},t)=\sum_{P=0}^{N-1}\sum_{j=1}^{n_{dof}}\sum_{\lambda\in\eta-\eta_{gj}}c_{Pj\lambda}^{(m)}\,\psi_\lambda(\mathbf{X})\cos(\frac{P\pi t}{T})\mathbf{e}_j,\\&c_{Pj\lambda}^{(0)}=0,\end{aligned}\tag{4.2}$$

and

$$\Delta\boldsymbol{\mathscr{Y}}^{pa^h(m)}(\mathbf{x},t)=\sum_{P=0}^{N-1}\sum_{j=1}^{n_{dof}}\sum_{\lambda\in\eta-\eta_{gj}}\Delta c_{Pj\lambda}^{(m)}\,\psi_\lambda(\mathbf{X})\cos(\frac{P\pi t}{T})\mathbf{e}_j.\tag{4.3}$$

$\Delta\boldsymbol{\mathscr{V}}^{pa^h(m)}$, $m=0,...,\mathscr{L}-1$, denotes the m^{th} displacement increment added to the m^{th} iteration, $\boldsymbol{\mathscr{V}}^{pa^h(m)}$. Also, $\mathscr{L}$ indicates the total number of iterations in each time-step. Now, by performing a linearization, after some manipulations, one can write for m^{th} iteration:

$$\begin{aligned}
&\int_{\mathscr{B}^0}\rho_0\left[\Delta\mathscr{V}_i^{pa^h(m)}*w_i\right](\mathbf{X},T)d\mathscr{B}\\
&+\int_{\mathscr{B}^0}\left[t*D^{(m)}F_{iQ}(\boldsymbol{\mathscr{X}}^{pa^h}(\mathbf{X},T))S_{QJ}(\boldsymbol{\mathscr{X}}^{pa^h}(\mathbf{X},T))*w_{i,J}\right](\mathbf{X},T)d\mathscr{B}\\
&+\int_{\mathscr{B}^0}\left[t*F_{iQ}(\boldsymbol{\mathscr{X}}^{pa^h}(\mathbf{X},T))D^{(m)}S_{QJ}(\boldsymbol{\mathscr{X}}^{pa^h}(\mathbf{X},T))*w_{i,J}\right](\mathbf{X},T)d\mathscr{B}\\
&+\mathscr{R}^{pa(m)}(\mathbf{w}(\mathbf{X},t))\Big|_{t=T}=0,
\end{aligned}\tag{4.4}$$

where

$$\begin{aligned}
\mathscr{R}^{pa(m)}(\mathbf{w}(\mathbf{x},t))\Big|_{t=T}&=\int_{\mathscr{B}^0}\rho_0\left[\mathscr{V}_i^{pa^h(m)}*w_i\right](\mathbf{X},T)d\mathscr{B}\\
&\int_{\mathscr{B}^0}\left[t*F_{iI}(\boldsymbol{\mathscr{X}}^{pa^h}+\boldsymbol{\mathscr{V}}^{pa^h(m)})S_{IJ}(\boldsymbol{\mathscr{X}}^{pa^h}+\boldsymbol{\mathscr{V}}^{pa^h(m)})*w_{i,J}\right](\mathbf{X},T)d\mathscr{B}\\
&-\int_{\partial\mathscr{B}^0_{t_i}}\left[t*\mathscr{H}_i^{pa}*w_i\right](\mathbf{X},T)d\Gamma-\int_{\mathscr{B}^0}\left[t*\rho b_i^{pa}*w_i\right](\mathbf{X},T)d\mathscr{B},
\end{aligned}\tag{4.5}$$

$$D^{(m)}\square_{\alpha\beta}(\boldsymbol{\mathscr{X}}^{pa^h}(\mathbf{X},T))=\left.\frac{d\square_{\alpha\beta}(\varepsilon\Delta\boldsymbol{\mathscr{V}}^{(m)}+\boldsymbol{\mathscr{X}}^{pa^h}(\mathbf{X},T))}{d\varepsilon}\right|_{\varepsilon=0},$$

$\square_{\alpha\beta}$ $(\alpha,\beta=1,2,3)$ denotes the components of a second-order tensor. It should be mentioned that while $t=T$ has been utilized in $(4.5)_2$ for $\boldsymbol{\mathscr{X}}^{pa^h}$, any time in the range of $0\leqslant t\leqslant T$ may be used provided that the corresponding Newton-Raphson procedure converges. Clearly, the above equation is a linear integral form in terms of $\Delta\boldsymbol{\mathscr{V}}^{pa^h(m)}$. In particular, a classical practice shows that equation (4.4) can be simplified as:

$$\begin{aligned}
&\int_{\mathscr{B}^0}\rho_0\left[\Delta\mathscr{V}_i^{(m)}*w_i\right](\mathbf{X},T)d\mathscr{B}+\int_{\mathscr{B}^0}\left[t*\Delta\mathscr{V}_{i,Q}^{(m)}S_{QJ}(\boldsymbol{\mathscr{X}}^{pa^h}(\mathbf{X},T))*w_{i,J}\right](\mathbf{X},T)d\mathscr{B}\\
&+2\int_{\mathscr{B}^0}\left[t*F_{iI}(\boldsymbol{\mathscr{X}}^{pa^h}(\mathbf{X},T))\mathscr{D}_{IJKL}\Delta\mathscr{V}_{j,K}^{(m)}F_{jL}(\boldsymbol{\mathscr{X}}^{pa^h}(\mathbf{X},T))*w_{i,J}\right](\mathbf{X},T)d\mathscr{B}\\
&+\mathscr{R}^{pa(m)}(\mathbf{w}(\mathbf{X},t))\Big|_{t=T}=0,
\end{aligned}\tag{4.6}$$

with

$$\mathscr{D}_{IJKL}=\left.\frac{\partial S_{IJ}}{\partial C_{KL}}\right|_{\mathbf{C}=\mathbf{F}^T(\boldsymbol{\mathscr{X}}^{pa^h}(\mathbf{X},T))\mathbf{F}(\boldsymbol{\mathscr{X}}^{pa^h}(\mathbf{X},T))},\tag{4.7}$$

and the fourth-order tensor $\mathscr{D}_{IJKL}$ has both minor and major symmetries. Now, employing (4.3) and (3.19) in (4.6), after some manipulations, we can write:

$$\begin{aligned}
&\sum_{\mathscr{P}=0}^{N-1}\sum_{j=1}^{n_{dof}}\sum_{\lambda\in\eta-\eta_{gj}}\mathscr{F}_{\mathscr{P}\mathscr{Q}}\Delta c_{Pj\lambda}^{(m)}(\rho_0\psi_\lambda(\mathbf{X})\mathbf{e}_j,\psi_\beta(\mathbf{X})\mathbf{e}_i)_{\mathscr{B}}+\sum_{\mathscr{P}=0}^{N-1}\sum_{j=1}^{n_{dof}}\sum_{\lambda\in\eta-\eta_{gj}}\mathscr{A}_{\mathscr{P}\mathscr{Q}}\Delta c_{Pj\lambda}^{(m)}a(\psi_\lambda\mathbf{e}_j,\psi_\beta(\mathbf{X})\mathbf{e}_i)_S\\
&+\sum_{\mathscr{P}=0}^{N-1}\sum_{j=1}^{n_{dof}}\sum_{\lambda\in\eta-\eta_{gj}}2\mathscr{A}_{\mathscr{P}\mathscr{Q}}\Delta c_{Pj\lambda}^{(m)}a(\psi_\lambda\mathbf{e}_j,\psi_\beta\mathbf{e}_i)_{\mathscr{D}}+\mathscr{R}^{pa(m)}(\mathbf{w}(\mathbf{X},t))\Big|_{t=T}=0,\\
&(i=1,..,n_{dof}),(\mathscr{Q}=0,...,N-1),\quad(\beta\in\eta-\eta_{gi}),
\end{aligned}\tag{4.8}$$

where the following notations were used:

$$\begin{aligned}
&(\mathbf{u},\mathbf{v})_{\mathscr{B}}=\int_{\mathscr{B}^0}\rho_0u_iv_id\mathscr{B},\ a(\mathbf{u},\mathbf{v})_S=\int_{\mathscr{B}^0}u_{i,I}\hat{S}_{IJ}v_{i,J}d\mathscr{B},\ a(\mathbf{u},\mathbf{v})_{\mathscr{D}}=\int_{\mathscr{B}^0}\hat{F}_{iI}u_{i,J}\mathscr{D}_{IJKL}\hat{F}_{jK}v_{j,L}d\mathscr{B},\\
&\hat{\mathbf{F}}=\mathbf{F}(\boldsymbol{\mathscr{X}}^{pa^h}(\mathbf{X},T)),\ \hat{\mathbf{S}}=\mathbf{S}(\boldsymbol{\mathscr{X}}^{pa^h}(\mathbf{X},T)),
\end{aligned}\tag{4.9}$$

$$\mathscr{A}_{\mathscr{P}\mathscr{Q}} = t*\cos(\frac{\mathscr{P}\pi t}{T})*\cos(\frac{\mathscr{Q}\pi t}{T})\Big|_{t=T} = \begin{cases} \frac{T^3}{\mathscr{P}^2\pi^2} & \mathscr{P}\neq 0, \mathscr{Q}=0 \\ \frac{T^3}{\mathscr{Q}^2\pi^2} & \mathscr{P}=0, \mathscr{Q}\neq 0 \\ (-1)^{\mathscr{P}+1}\frac{T^3}{2\mathscr{P}^2\pi^2} & \mathscr{P}=\mathscr{Q}\neq 0 \\ \frac{T^3}{6} & \mathscr{P}=\mathscr{Q}=0 \\ 0 & otherwise \end{cases},$$

$$\mathscr{F}_{\mathscr{P}\mathscr{Q}} = \cos(\frac{\mathscr{P}\pi t}{T})*\cos(\frac{\mathscr{Q}\pi t}{T})\Big|_{t=T} = \begin{cases} (-1)^{\mathscr{P}}\frac{T}{2} & \mathscr{P}=\mathscr{Q}\neq 0 \\ T & \mathscr{P}=\mathscr{Q}=0 \\ 0 & otherwise \end{cases}.$$

Having solved (4.8), one can obtain $\boldsymbol{\mathscr{V}}^{pa^h(m+1)}(\mathbf{x},t)$ from $(4.1)_1$.

5 Properties of Solution Procedure

The convolution solver inherits the desirable characteristics of time-space decoupled and coupled finite element methods. In other words, as explained in [19], this solver follows the same straightforward steps relevant to time integration methods while stemming from a coupled space-time integral. Herein by saying the same 'step,' we mean in the convolution solver, analogous to the time integration methods, the spatial discretization can be initially done and then the associated nonlinear ODEs are solved. To explain properties of the new method, we first explain some facts regarding semi-discrete equations of motion obtained from (2.1). The formulation is represented only for one time sub-interval which should be applied consecutively with updated initial data and external force to find the solution for any desired time interval. In doing so, after spatial discretization, one obtains the following evolutionary nonlinear ODEs and initial conditions:

$$\begin{aligned} &[\mathbf{M}]\left[\ddot{\mathbf{U}}(t)\right]+[\mathbf{K}([\mathbf{U}(t)])]=[\mathbf{f}(t)],\ 0\leqslant t\leqslant T \\ &[\mathbf{U}(0)]=[\mathbf{U}_0],\left[\dot{\mathbf{U}}(0)\right]=\left[\dot{\mathbf{U}}_0\right], \end{aligned} \tag{5.1}$$

5.1 New Method

Considering (5.1), the corresponding alternative governing equations read:

$$[\mathbf{M}][\mathbf{V}(t)]+t*\left[\mathbf{K}([\mathbf{V}(t)]+[\mathbf{U}_0]+t\left[\dot{\mathbf{U}}_0\right])\right]-t*[\mathbf{f}(t)]=[\mathbf{0}],\ 0\leqslant t\leqslant T \tag{5.2}$$

where

$$[\mathbf{V}(t)]=[\mathbf{U}(t)]-[\mathbf{U}_0]-t\left[\dot{\mathbf{U}}_0\right]. \tag{5.3}$$

The set of nonlinear ODEs (5.2) is equivalent to:

$$\left([\mathbf{M}][\mathbf{V}(t)]+t*\left[\mathbf{K}([\mathbf{V}(t)]+[\mathbf{U}_0]+t\left[\dot{\mathbf{U}}_0\right])\right]-t*[\mathbf{f}(t)]\right)*\cos(\frac{Q\pi t}{T})\Big|_{t=T}=[\mathbf{0}],\ Q=0,...,\infty, \tag{5.4}$$

in the sense that the following norm is vanished:

$$\left|[\mathbf{M}][\mathbf{V}(t)]+t*\left[\mathbf{K}([\mathbf{V}(t)]+[\mathbf{U}_0]+t\left[\dot{\mathbf{U}}_0\right])\right]-t*[\mathbf{f}(t)]\right|^2=0. \tag{5.5}$$

In the numerical implementations, the notion of inifinity in the above equation is realized by considering a large number, say $N-1$. Now, following the similar manupulations represented in [24], one can find the m^{th} iteration, which is equivalent to (4.4), as follows:

$$[\mathbf{M}]\left[\sum_{P=0}^{N-1}\left(\Delta[\mathbf{c}]_P^{(m)}\right)\cos\left(\frac{P\pi t}{T}\right)\right]*\cos\left(\frac{Q\pi t}{T}\right)\Big|_{t=T}+t*[D\mathbf{K}]\cdot\left[\sum_{P=0}^{N-1}\left(\Delta[\mathbf{c}]_P^{(m)}\right)\cos\left(\frac{P\pi t}{T}\right)\right]*\cos\left(\frac{Q\pi t}{T}\right)\Big|_{t=T}+$$
$$[\mathbf{R}]^{(m,Q)}=[\mathbf{0}],\ Q=0,...,N-1. \tag{5.6}$$

with:

$$[\mathbf{R}]^{(m,Q)}=\left([\mathbf{M}][\mathbf{V}(t)]^{(m)}+t*\left[\mathbf{K}([\mathbf{V}(t)]^{(m)}+[\mathbf{U}_0]+t\left[\dot{\mathbf{U}}_0\right])\right]-t*[\mathbf{f}(t)]\right)*\cos\left(\frac{Q\pi t}{T}\right)\Big|_{t=T}, \tag{5.7}$$

in which $[D\mathbf{K}]$ represents the consistent tangent matrix. The above equations can be written in the matrix form as:

$$\begin{bmatrix} \mathscr{F}_{00}[\mathbf{M}]+\mathscr{A}_{00}[D\mathbf{K}] & \mathscr{A}_{01}[D\mathbf{K}] & & \cdots & & & \mathscr{A}_{0N}[D\mathbf{K}] \\ \mathscr{A}_{01}[D\mathbf{K}] & \mathscr{F}_{11}[\mathbf{M}]+\mathscr{A}_{11}[D\mathbf{K}] & \mathbf{0} & \cdots & & & \mathbf{0} \\ \vdots & \vdots & \ddots & \vdots & & & \vdots \\ \mathscr{A}_{0r}[D\mathbf{K}] & \mathbf{0} & \cdots & \mathscr{F}_{rr}[\mathbf{M}]+\mathscr{A}_{rr}[D\mathbf{K}] & \mathbf{0} & \cdots & \mathbf{0} \\ \vdots & \vdots & & \vdots & \ddots & & \end{bmatrix} \begin{bmatrix} [\Delta\mathbf{c}]_0^{(m)} \\ [\Delta\mathbf{c}]_1^{(m)} \\ \vdots \\ [\Delta\mathbf{c}]_r^{(m)} \\ \vdots \end{bmatrix} = - \begin{bmatrix} [\mathbf{R}]^{(m,0)} \\ [\mathbf{R}]^{(m,1)} \\ \vdots \\ [\mathbf{R}]^{(m,r)} \\ \vdots \end{bmatrix}, \tag{5.8}$$

where the left hand side is an arrowhead block matrix. This matrix form paves the way for considering an arbitrary number of time-wise terms while maintaining the computational cost affordable. More specifically, to obtain the inverse of the large matrix given in (5.8), one can write $[\Delta\mathbf{c}]_r^{(m)}$, $r=1,...N-1$, in terms of $[\Delta\mathbf{c}]_0^{(m)}$, calculating $[\Delta\mathbf{c}]_0^{(m)}$ from the first set of equations. Then, the other $[\Delta\mathbf{c}]_r^{(m)}$, $r=1,...N-1$, can be computed by knowing $[\Delta\mathbf{c}]_0^{(m)}$. Apparently, this procedure is suitbale for paralell programming as most of the calculations are performed indepentenly. Moreover, based on previous explanations, the linear solver is similar to time integration methods while, as analyzed in [19], achieving accurate solution for any time span.

The new solution procedure has three parameters: 1) number of time-wise terms, N 2) number of time-steps, N_s 3) the parameter, γ, $0<\gamma<1$. As mentioned earlier, the time-step in this method is $\Delta t=(1-\gamma)T$. Hence, in this method $u(\mathbf{x},s\Delta t)$, $\dot{u}(\mathbf{x},s\Delta t)$ $(s=0,...,N_s-1)$ are used as initial values for $(s+1)^{th}$ step. It is observed that for the same Δt the larger T, the lesser γ needs to be selected. It should be mentioned that it is required to define γ in this method since, regardless of the choice of N, the resulting solution does not converge to the exact values at $t=T$ (see [19]). The main steps of the new solution procedure have been represented in the algorithms 1 & 2. In these algorithms $\mathbf{u}^0_{FEM}$, $\mathbf{v}^0_{FEM}$, $\mathbf{u}^b_{FEM}$, $\boldsymbol{t}^b_{FEM}$, and $\mathbf{f}_{FEM}$, respectively, denote the contribution due to initial displacement, initial velocity, displacement boundary conditions, traction boundary conditions, and body forces.

The evaluation of residuals is a significant step in this method. As can be seen, contrary to classical forms, the residuals in this approach involve both spatial and temporal integrals. In this respect, quadrature methods, e.g., Gauss-Legendre, can be employed to deal with such integrals. However, given that the Newton-Raphson approach converges, for large values of time step T, evaluating the integrals with quadrature methods could be an uphill task. But, this problem can be efficiently alleviated by the method initially introduced in [27]. The temporal integrals of the residuals has the following form:

$$\int_0^T f(t)\cos(\omega t)dt. \tag{5.9}$$

This type of integrals can be approximated by using [28]:

$$\int_{-1}^{1} f(t)e^{i\omega t}dt \approx \left(\frac{\pi}{2\omega}\right)^{1/2} \int_{-1}^{1} f(x) \sum_{\kappa=1}^{r} (2\kappa+1) i^{\kappa} J_{\kappa+\frac{1}{2}}(\omega) P_{\kappa}(t)dt, \tag{5.10}$$

or

$$\int_{-1}^{1} f(t)\cos(\omega t)dt = \left(\frac{\pi}{2\omega}\right)^{1/2} \int_{-1}^{1} f(t) \sum_{\kappa=1}^{\lceil r/2 \rceil} (2\kappa+1)(-1)^{\kappa} J_{2\kappa+\frac{1}{2}}(\omega) P_{2\kappa}(t)dt, \tag{5.11}$$

in which J_α and P_α denote Bessel functions of the first kind of order α and Legendre functions of order α, respectively. Now, the right-hand-side of (5.10) and (5.11) can be calculated by applying r-points Gaussian quadrature rule, where it is exact when $f(t)$ is a polynomial of order r [28]. The merit of (5.10) (or (5.11)) is that the major part of computation for this category of problems is performed and saved once for all computations, reducing the amount of calculations considerably. As another approach, one can also approximate the Fourier cosine expansion of the corresponding integrand with the Fast Fourier Transform (FFT) algorithm. Having found the Fourier cosine expansion, one can straightforwardly evaluate such integrals with the aid of $(4.9)_3$. It should be noticed that the larger T, the more sample points for FFT algorithm are required.

Algorithm 1: Nonlinear Dynamic Finite Element Scheme

Define N, N_s, γ, tolerance, and T^{total};
$T \leftarrow \frac{T^{total}}{N_s(1-\gamma)}$;
Calculate $[\mathscr{A}]$, $[\mathscr{F}]$ from (4.9)$_{3-4}$;
Define appropriate spatial shape functions;
Assign initial and boundary conditions and body forces in the matrix form based on the spatial-temporal shape functions: $\mathbf{u}^0_{FEM}$, $\mathbf{v}^0_{FEM}$, $\mathbf{u}^b_{FEM}$, $\boldsymbol{t}^b_{FEM}$, $\mathbf{f}_{FEM}$;
Calculate $[\mathbf{M}]$;
for $l = 1 : N_s$ **do**
  Calculate $[D\mathbf{K}]$
    CNRS ($[\mathbf{M}]$, $[D\mathbf{K}]$, $\mathbf{u}^0_{FEM}$, $\mathbf{v}^0_{FEM}$, $\mathbf{u}^b_{FEM}$, $\boldsymbol{t}^b_{FEM}$, $\mathbf{f}_{FEM}$, $[\mathscr{A}]$, $[\mathscr{F}]$, N, T,γ, l, tolerance)
    return $[\mathbf{U}]$, $[\dot{\mathbf{U}}]$;
      $[\mathbf{U}]_l \leftarrow [\mathbf{U}]$, $\mathbf{u}^0_{FEM} \leftarrow [\mathbf{U}]$;
      $[\dot{\mathbf{U}}]_l \leftarrow [\dot{\mathbf{U}}]$, $\mathbf{v}^0_{FEM} \leftarrow [\dot{\mathbf{U}}]$;
end

Algorithm 2: Convolution-Newton-Raphson Solver (CNRS) ($[\mathbf{M}]$, $[D\mathbf{K}]$, $\mathbf{u}^0_{FEM}$, $\mathbf{v}^0_{FEM}$, $\mathbf{u}^b_{FEM}$, $\boldsymbol{t}^b_{FEM}$, $\mathbf{f}_{FEM}$, $[\mathscr{A}]$, $[\mathscr{F}]$,T, N, γ, l, tolerance)

$[\mathbf{c}]^{(0)}_r \leftarrow [\mathbf{0}]$, $r = 0,...,N-1$;
id=tolerance+1;
$m \leftarrow 0$;
while $id > tolerance$ **do**
  compute $[\mathbf{R}]^{(m,r)}$, $r = 0,...,N-1$, based on $\mathbf{u}^0_{FEM}$, $\mathbf{v}^0_{FEM}$, $\mathbf{u}^b_{FEM}$, $\boldsymbol{t}^b_{FEM}$, and $\mathbf{f}_{FEM}$ for $t = T$ and l;
  Obtain $[\Delta\mathbf{c}]^{(m)}_0$ from (5.8) ;
  $[\Delta\mathbf{c}]^{(m)}_r \leftarrow (\mathscr{F}_{rr}[\mathbf{M}] + \mathscr{A}_{rr}[D\mathbf{K}])^{-1}([\mathbf{R}]^{(m,r)} - \mathscr{A}_{0r}[D\mathbf{K}][\Delta\mathbf{c}]^{(m)}_0)$, $r = 0,...,N-1$;
  $[\mathbf{c}]^{(m+1)}_r \leftarrow [\mathbf{c}]^{(m)}_r + [\Delta\mathbf{c}]^{(m)}_r$, $r = 0,...,N-1$;
  $[\mathbf{R}]^{(m+1)} \leftarrow \left[[\mathbf{R}]^{(m+1,1)^T},...,[\mathbf{R}]^{(m+1,N-1)^T}\right]^T$;
  $id = [\mathbf{R}]^{(m+1)}[\mathbf{R}]^{T(m+1)}$;
  $m \leftarrow m+1$;
end
return $[\mathbf{U}((1-\gamma)T)] = [\mathbf{V}((1-\gamma)T)]^{(m-1)} + [\mathbf{u}^0] + (1-\gamma)T[\mathbf{v}^0]$;
return $[\dot{\mathbf{U}}((1-\gamma)T)] = [\dot{\mathbf{V}}((1-\gamma)T)]^{(m-1)} + [\mathbf{v}^0]$;

6 Numerical Results

6.1 Free Vibration

In this part, several aspects of the new approach are considered. To highlight the characteristics of the new method, in some figures, we also show the same results corresponding to the average acceleration method. For the Nemwark method, we follow the formulation given in [1]: in this method, (5.1) is satisfied at discrete time instances $t_1 = \Delta t,...,t_n = n\Delta t$ with Δt, representing the time-step. Denoting $[\mathbf{U}(t_n)] \approx [\mathbf{U}_n]$, $[\dot{\mathbf{U}}(t_n)] \approx [\dot{\mathbf{U}}_n]$, and $[\ddot{\mathbf{U}}(t_n)] \approx [\ddot{\mathbf{U}}_n]$, one solves the following equations with Newton-Raphson method [1]:

$$\frac{4}{\Delta t^2}[\mathbf{M}][\mathbf{U}_{n+1}] + [\mathbf{K}(\mathbf{U}_{n+1})] = [\mathbf{f}_{n+1}] + [\mathbf{G}_{n+1}] \tag{6.1}$$

with

$$
\begin{aligned}
[\mathbf{G}_{n+1}] &= \frac{4}{\Delta t^2}[\mathbf{M}][\mathbf{U}_n] + \frac{4}{\Delta t}[\mathbf{M}][\dot{\mathbf{U}}_n] + [\mathbf{M}][\ddot{\mathbf{U}}_n] \\
[\dot{\mathbf{U}}_{n+1}] &= \frac{2}{\Delta t}([\mathbf{U}_{n+1}] - [\mathbf{U}_n]) - [\dot{\mathbf{U}}_n], \\
[\ddot{\mathbf{U}}_{n+1}] &= \frac{2}{\Delta t}([\dot{\mathbf{U}}_{n+1}] - [\dot{\mathbf{U}}_n]) - [\ddot{\mathbf{U}}_n], \quad [\ddot{\mathbf{U}}_0] = [\mathbf{M}]^{-1}([\mathbf{f}_0] - [\mathbf{K}(\mathbf{U}_0)]),
\end{aligned}
\tag{6.2}
$$

where the initial values are considered for the case $n = 0$.
First, the free vibration of an elastic plate under initial displacement and velocity is considered. Two constitutive models are utilized: Neo-Hookean and Saint Venant–Kirchhoff models. The potential energy function for the Neo-Hookean model is:

$$
W(\mathbf{C}) = \frac{\lambda}{2}\log^2\left(\sqrt{\det\mathbf{C}}\right) + \frac{\mu}{2}(\mathrm{tr}(\mathbf{C}) - 3) - \mu\log\left(\sqrt{\det\mathbf{C}}\right), \tag{6.3}
$$

while the potential energy function relevant to the Saint Venant-Kirchhoff model, which is the extension of linear Hook's Law that incorporates geometrical nonlinearity, is:

$$
W(\mathbf{C}) = \frac{\lambda}{2}\left(\mathrm{tr}\left(\frac{\mathbf{C}-\mathbf{I}}{2}\right)\right)^2 + \mu\,\mathrm{tr}\left(\frac{\mathbf{C}-\mathbf{I}}{2}\right)^2. \tag{6.4}
$$

The geometry of the plate is shown in Fig. 2a, with $a = 1.0m$ and $h = 1.0m$. In the simulations, $\mu = 1.2\times10^8\,\frac{N}{m^2}$, $\lambda = 1.2\times10^8\,\frac{N}{m^2}$ and $\rho_0 = 770\,\frac{Kg}{m^3}$ is considered. Linear Lagrange shape functions are used with uniform quadrilateral elements. For most cases, the geometry of the problem is approximated in terms of 10×10 uniform mesh. However, other mesh arrangements (e.g., 5×5 uniform mesh) are employed to calculate other quantities such as the error estimation. The following initial conditions are exerted, respectively, on the Saint Venant-Kirchhoff and the Neo-Hookean plates:

$$
\begin{aligned}
&u_1(X_1,X_2,0) = 0,\ u_2(X_1,X_2,0) = \begin{cases} 0 & X_1 = 0 \\ 0.1X_2 & X_1 \neq 0 \end{cases}, \\
&\dot{u}_1(X_1,X_2,0) = \begin{cases} 0 & X_1 = 0 \\ 100X_1 & X_1 \neq 0 \end{cases},\ \dot{u}_2(X_1,X_2,0) = 0.
\end{aligned}
\tag{6.5}
$$

$$
\begin{aligned}
&u_1(X_1,X_2,0) = 0,\ u_2(X_1,X_2,0) = \begin{cases} 0 & X_1 = 0 \\ 0.2X_2 & X_1 \neq 0 \end{cases}, \\
&\dot{u}_1(X_1,X_2,0) = \begin{cases} 0 & X_1 = 0 \\ 200X_1 & X_1 \neq 0 \end{cases},\ \dot{u}_2(X_1,X_2,0) = 0.
\end{aligned}
\tag{6.6}
$$

The top right corner of the plate with coordinate $\mathbf{X}^{ref} = (L,L)$ is selected as the reference point for producing the numerical results. Also, the reference solution in this study is mainly the one resulting from the trapezoidal rule with a small time-step (for most cases, we considered $\Delta t = {}^{T^{total}}/_{3,000}$). Also, to highlight the capability of the new algorithm, the data resulting from the average acceleration method with the same time-step size employed for the present study is reported. Since the Newton-Raphson method is used to deal with the nonlinear problem, the time-step version of the CFEM is applied (see [19]). In particular, the total time interval is divided into smaller sub-intervals $T = T^{total}/(N_s(1-\gamma))$, in which N_s represents the number of sub-intervals, and γ is a parameter to circumvent the non-convergence nature of the linear solver due to cosine expansion [19]. Then, as mentioned earlier, the results at the time instances $s\Delta t = s(1-\gamma)T$, $s = 1,\ldots,N_s$, are reported.
In Figs. 3 and 4, the vertical and horizontal displacement and velocity of the reference point are shown using the time-span of $T = T^{total}/125$ ($N_s = 250$ and $\gamma = 0.5$) with $N = 50$ and $N = 200$. Although a good convergence for displacements attained through both methods, the robustness of the new method is recognizable in velocity profiles. In particular, in the velocity profile, the Newmark method with $\Delta t = T^{total}/250$ failed to converge to the reference solution, while an excellent match between the outputs of the new method and the reference solution is seen. This fact is attributed to the property of the linear solver that can capture the linear solution regardless of the time-step size. This property implies that the new solution procedure is equivalent to higher-order accurate time integration methods in the sense that the technique can adaptively capture the solution for larger time-steps provided that the corresponding Newton-Raphson algorithm is converged.
The deformed configuration at $t = 0.1s$ is shown in Fig. 5. To show that the problem incorporates nonlinear geometry, we report the engineering strain, Green-Lagrange strain, and their difference, respectively, in Figs. 6, 8, and 7. Fig. 6 infers that the condition for small strain theory, $\|\nabla\mathbf{u}\| \ll 1$, is no longer valid in this example. This fact can also be concluded from the comparison of Figs. 6 and 7, which shows the magnitude of the strain due to the nonlinear term is the same as the engineering strain.

Furthermore, the spatial variation of displacement, velocity, and stress fields are illustrated at $t = T^{total}$ using 100 elements, 200 time-wise terms, $N_s = 250$ and $\gamma = 0.5$ in Figs. 9-11. These figures confirm the satisfaction of the defined displacement boundary conditions. Also, compared to displacement fields, more fluctuations are noticed in the velocity and stress fields, a similar fashion typically discerned in the linear regime.

For the subsequent analysis, the Saint Venant–Kirchhoff model, with the potential function (6.4), is utilized as the constitutive equations. In Figs. 12 and 13, the vertical and horizontal velocities are depicted for this material through the proposed method ($N_s = 100$, 150 and $\gamma = 0.5$). The excellent performance of the CFEM linear solver is evident in recovering the Newmark method with the small Δt (i.e., the reference solution), showing the robustness of the proposed solution procedure in obtaining accurate results for larger time-steps.

Next, to quantify the error of the analysis, we employed the following error-index:

$$E^{index}(\mathbf{X}) = \sqrt{\frac{\int_0^T (u_R(\mathbf{X},t) - u_N(\mathbf{X},t))^2 dt}{\int_0^T u_R(\mathbf{X},t)^2 dt}}, \tag{6.7}$$

where $u_R(\mathbf{X},t)$ is a reference solution and $u_N(\mathbf{X},t)$ is the numerical solution. For the reference point, the displacement error versus the number of elements and time-wise terms is shown in Fig. 14. The reference solution here is the results corresponding to the analysis of 100 elements and $N = 200$. It can be observed that increasing the number of elements and N reduces the error. Also, the error-cap can be approximately achieved if $N = 200$ is selected.

Subsequently, the characteristics of the proposed method is explored through the conservation of the total energy. For different time-wise terms (with $N_s = 150$ and $\gamma = 0.5$), the variation of the total energy versus time is shown in Fig. 15. Apparently, by increasing the number of time-wise terms, the conservation of total energy can be fulfilled in a better manner. This demonstration confirms that, for a given time-step, the new algorithm can adaptively conserve energy in contrast to the Newmark method. It should be noted that the arrowhead block matrix appearing in the linear solver makes the calculation possible for large values of N, and thus, the adaptive nature of the new method is feasible.

To explore the effect of γ, we consider two cases, i.e., $\gamma = 0.2$ and $\gamma = 0.6$, and the resulting total energy is depicted for different N's (form $N = 200$ to $N = 10,000$) in Figs. 16a and 16b. It is observed that by increasing N, the CFEM solver can control the energy growth (decay) and obtain accurate results regardless of choice of γ. However, this goal is achieved with more computational costs. It is noted that choosing $0.5 \leq \gamma < 1$ entails larger values of N to find accurate results since a larger time-span T is required for the same Δt (see Fig. 16a). Also, by comparing Figs. 16a and 16b, one can recognize that the decay (growth) pattern of energy in the new method may alter depending on whether $0 < \gamma < 0.5$ or $0.5 < \gamma < 1$ is selected.

To better picture the capability of the method, we numerically show that the new method captures the nonlinear response of materials over a long range of time intervals. To this end, the conservation of energy, a critical property of any rigorous solution procedure, is evaluated for $T^{total} = 0.2s$ for Saint Venant-Kirchhoff plate (see Fig. 17). From this figure, it is observed that the trapezoidal rule falls short in conserving the energy, while for sufficiently large N's, the new method conserves the total energy.

Next, we compare the present algorithm with the energy-momentum method (E-M) developed in [7]. To this end, the free vibration of the Saint Venant-Kirchhoff plate is reconsidered. The total energy function has been computed using this method with small and large time-steps, the proposed method, and the average acceleration method with small and large time-steps (see Fig. 18). In this figure, the exact conservation of total energy has been satisfied using the energy-momentum algorithm regardless of the time-step size. In contrast, the present algorithm and the average acceleration method with the small time-step could achieve energy conservation numerically. The displacement and velocity values for the reference point have then been evaluated and depicted in Figs. 19 and 20. As expected, the proposed algorithm, even with a large time-step, closely follows the results corresponding to the energy-momentum algorithm with the small time-step. However, the adopted energy-momentum method with large time-step cannot recover the accurate solution (i.e., one with small-time steps). This result clearly show that, as opposed to the available time integration methods with finite order of the accuracy, by increasing N, the new method captures the exact solution for large time-steps.

6.2 Forced Vibration

Here we analyze the problem of the forced vibration of nonlinear materials. In this regard, a Neo-Hookean cantilever beam with the same-as-before earlier parameters is considered in Fig. 2b. The geometric characteristics of the beam are $a = 1m$ and $h = 0.1m$, and a uniform quadrilateral linear mesh of 20×2 is used for the discretization. Furthermore, a uniform pressure of $q = 2 \times 10^5 N/m^2$ is applied instantly on the beam and remains unchanged throughout the analysis. The top right corner of the beam is represented as the reference point for output calculations. By utilizing the CFEM solver ($N = 100, N_s = 1,000$ and $\gamma = 0.5$), the vertical and horizontal deformations of the reference point are displayed in Fig. 21 and compared with the trapezoidal rule using both large and small time steps. The corresponding velocity has

also been illustrated in Fig. 22. A slight differences between trapezoidal rule with large and small time-steps can be seen from these figures. A similar conclusion is observed from the figure: given that the corresponding Newton-Raphson method converges, the present method with larger Δt's captures accurately the results of the Newmark Method with small ones. Also, the deformed beam at $t = 0.1s$ ($t = 0.1 \times T^{total}$) is depicted in Fig. 23. This figure implies the presence of a contribution due to the geometrical nonlinearity in computations. To demonstrate this fact, we report the infinitesimal strain components and the difference between Green-Lagrange and infinitesimal strains at $t = 0.1s$ in Figs. 24 and 25. Also, the Green-Lagrange strain field are shown in 26. Clearly, the order of strain due to the nonlinear term and the infinitesimal strain tensor are in the same range, showing the necessity of employing the finite strain theory. Moreover, the displacement and velocity profiles of the beam are given in Figs. 27 and 28. Finally, the stress field variables are depicted in Fig. 29, showing the stress concentration at position of the Dirichlet boundary condition.

7 Concluding remarks

In this study, a novel solution procedure to deal with nonlinear elastodynamics has been proposed. The formulation has been presented for the large deformation theory where the nonlinearity comes from both constitutive equations and geometrical configuration. The results show that the method can successfully address the energy conservation issue existing in the trapezoidal method without further enforcing parameters such as Lagrange multipliers. In addition to that, the method is conspicuously versatile to obtain accurate results for larger time-steps, meaning that the method is a higher-order one in that sense. The main characteristics of the proposed algorithm are:

- The linear solver, i.e., the CFEM, does not require discretization in time, although it is rooted in a coupled space-time variational principle.
- The solution procedure is similar to the classical nonlinear dynamic finite element method where the Newmark average acceleration method is combined with the Newton-Raphson method but, in contradistinction to Newmark, can adaptively conserve the energy.
- As opposed to methods with finite order of accuracy, the algorithm is versatile to obtain accurate solution when increasing the time-step.
- From a computational perspective, the resultant block arrowhead matrix in (5.8) justifies the application of the method for nonlinear elastodynamics.
- The linear solver is suitable for parallel programming as most operations in the convolution-Newton-Raphson solver can be executed independently.

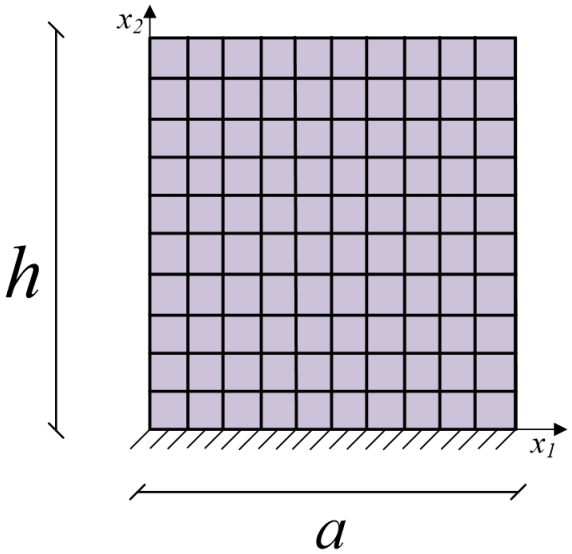

(a) Nonlinear plate.

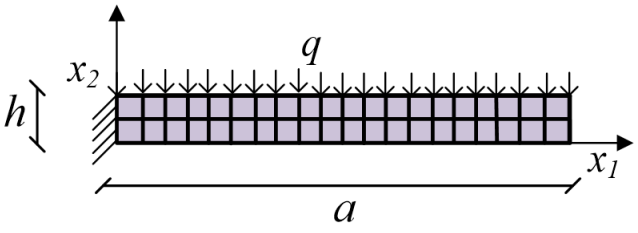

(b) Nonlinear beam.

Figure 2: The geometry of the problems.

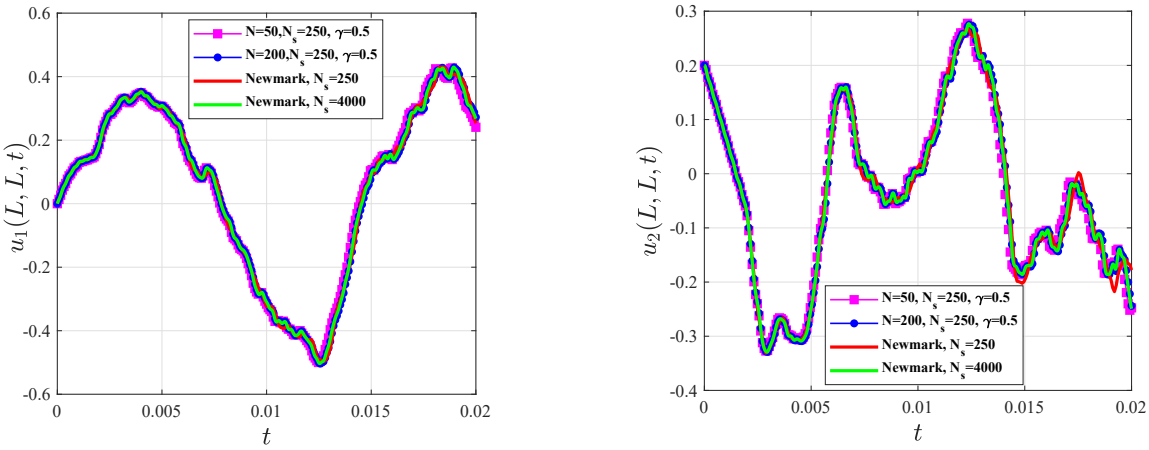

Figure 3: Horizontal and vertical displacement of the reference point for Neo-Hookean material ($T^{total} = 0.02s$).

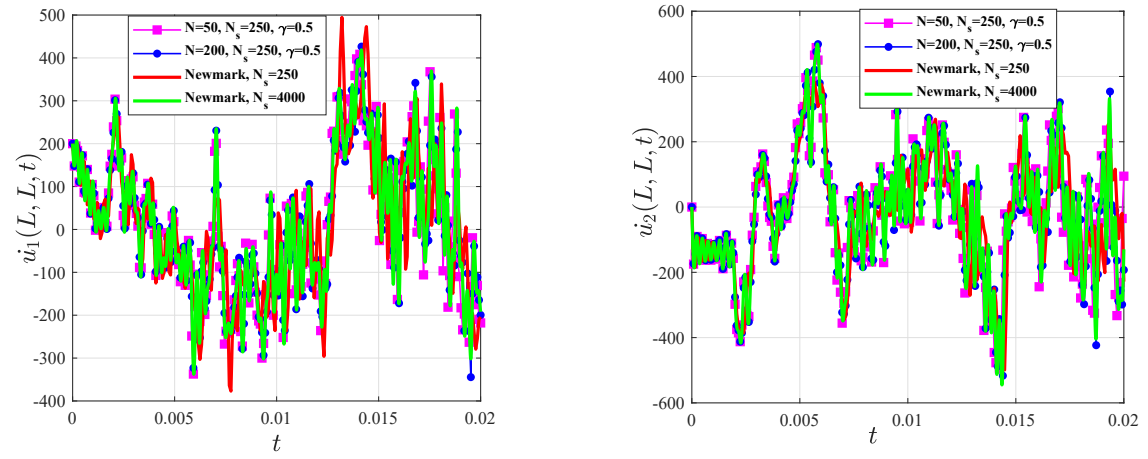

Figure 4: Horizontal and vertical velocity of the reference point for Neo-Hookean material ($T^{total} = 0.02s$).

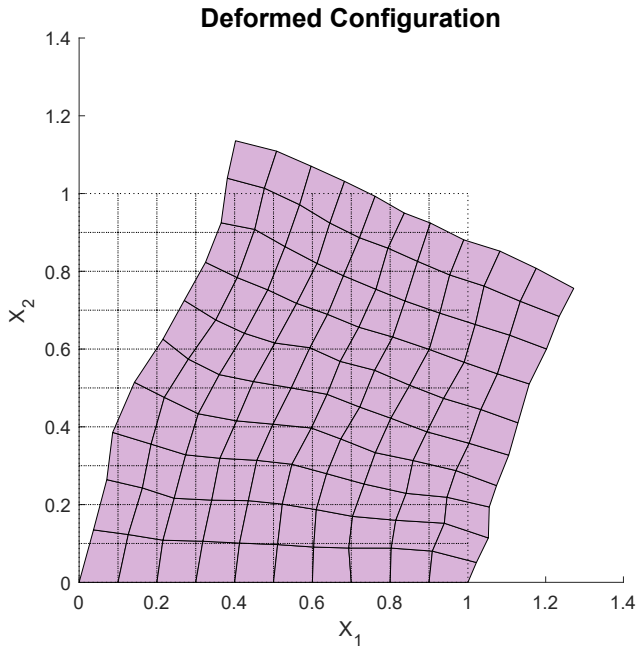

Figure 5: Deformed configuration of the Neo-Hookean plate at $t = T^{total}$ ($N_s = 250$ and $\gamma = 0.5$).

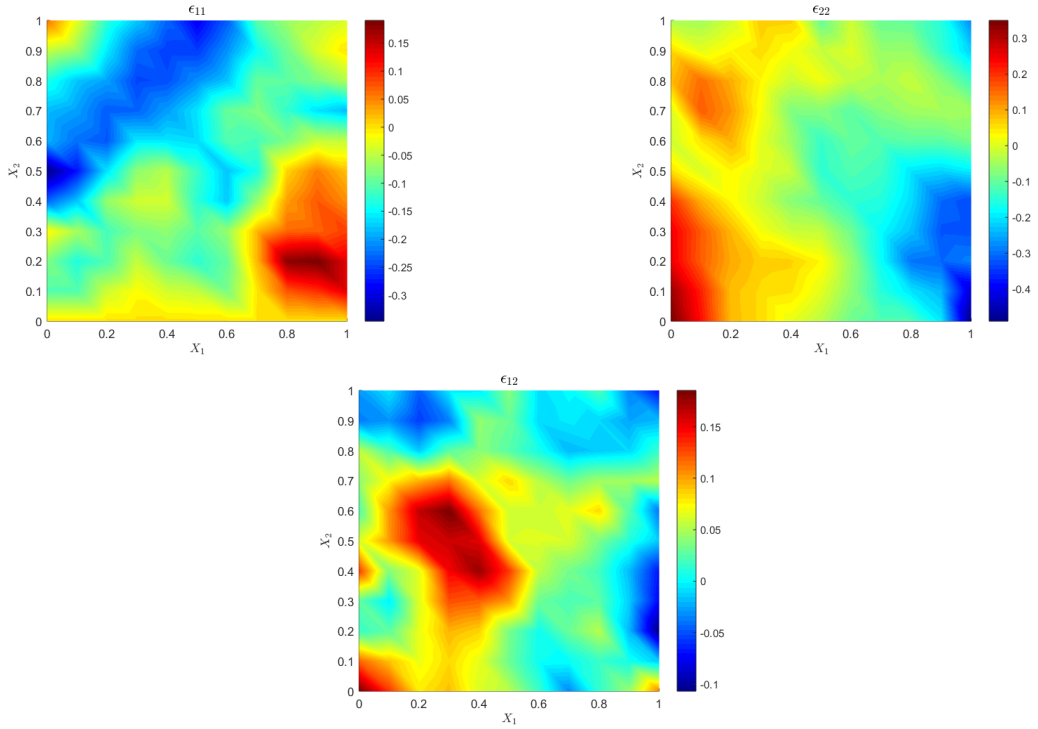

Figure 6: The infinitesimal strain components for the Neo-Hookean plate at $t = T^{total}$ ($N_s = 250$ and $\gamma = 0.5$).

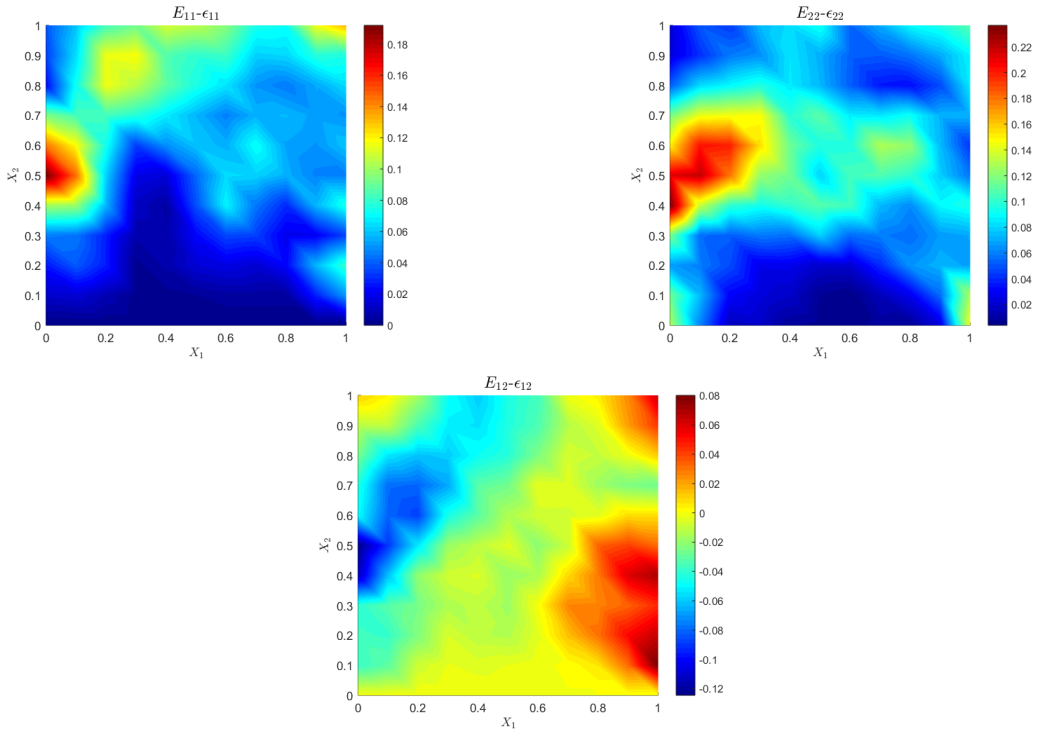

Figure 7: The Nonlinear parts of Green-Lagrange strain components for the Neo-Hookean plate at $t = T^{total}$ ($N_s = 250$ and $\gamma = 0.5$).

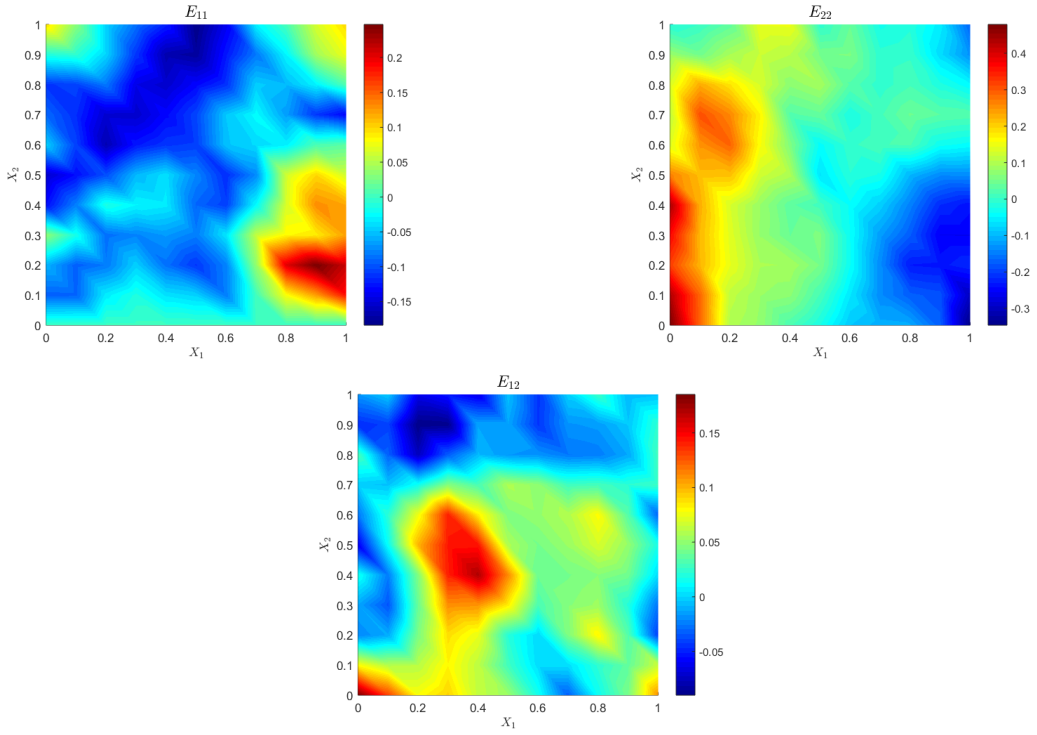

Figure 8: The Green-Lagrange strain components for the Neo-Hookean plate at $t = T^{total}$ ($N_s = 250$ and $\gamma = 0.5$).

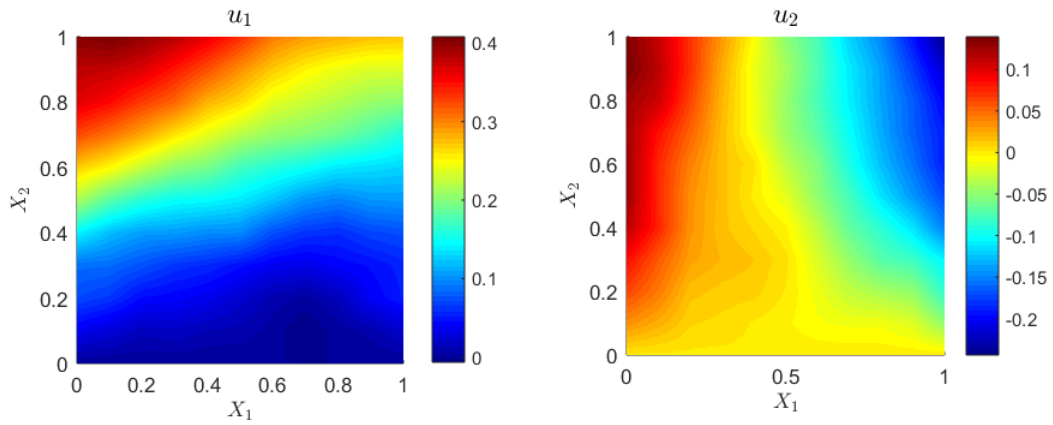

Figure 9: Horizontal and vertical displacement fields for the Neo-Hookean plate at $t = T^{total}$ ($N_s = 250$ and $\gamma = 0.5$).

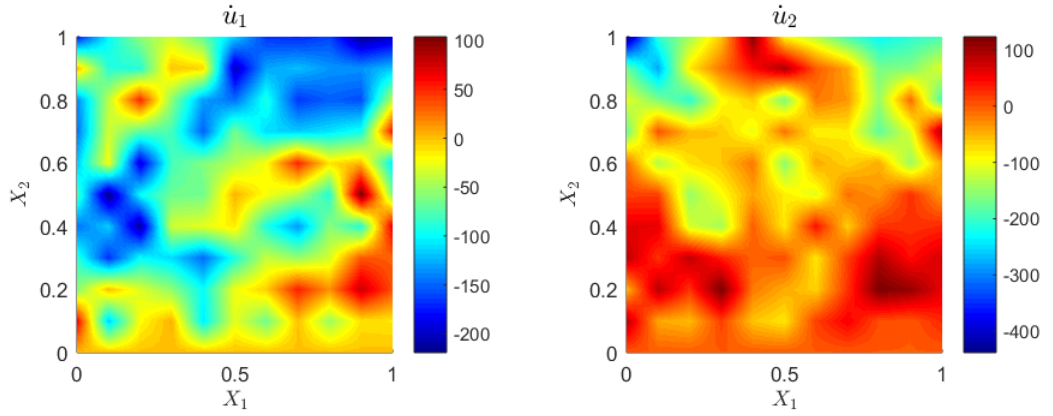

Figure 10: Horizontal and vertical velocity fields for the Neo-Hookean plate at $t = T^{total}$ ($N_s = 250$ and $\gamma = 0.5$).

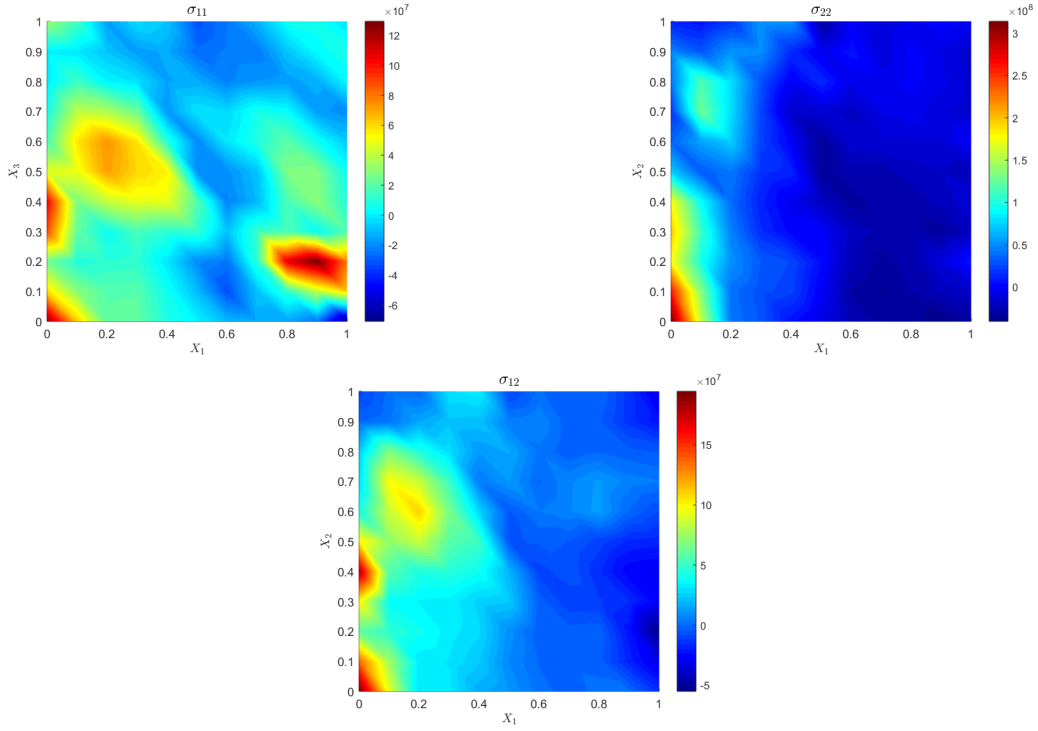

Figure 11: The stress components for the Neo-Hookean plate at $t = T^{total}$ ($N_s = 250$ and $\gamma = 0.5$).

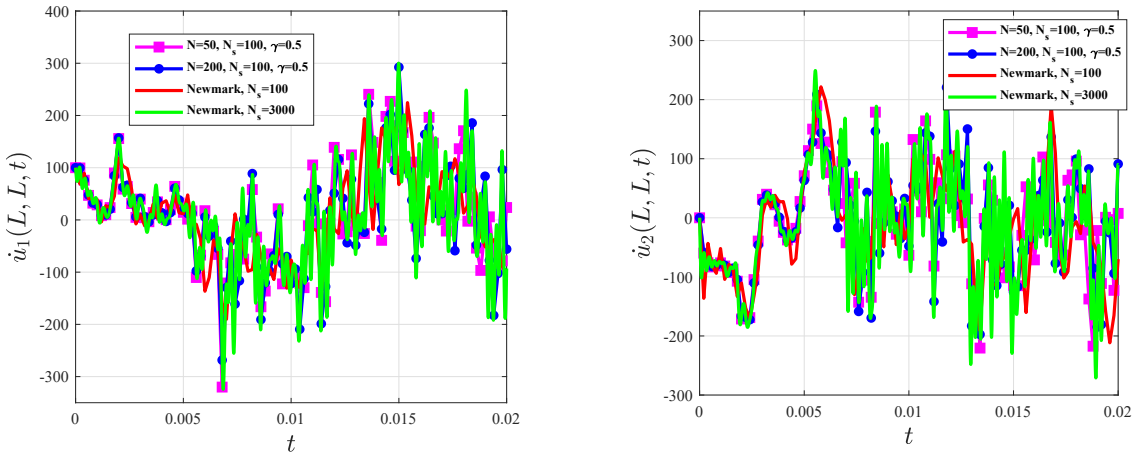

Figure 12: Horizontal and vertical velocity fields of the reference point for Saint Venant-Kirchhoff material ($T^{total} = 0.02s$).

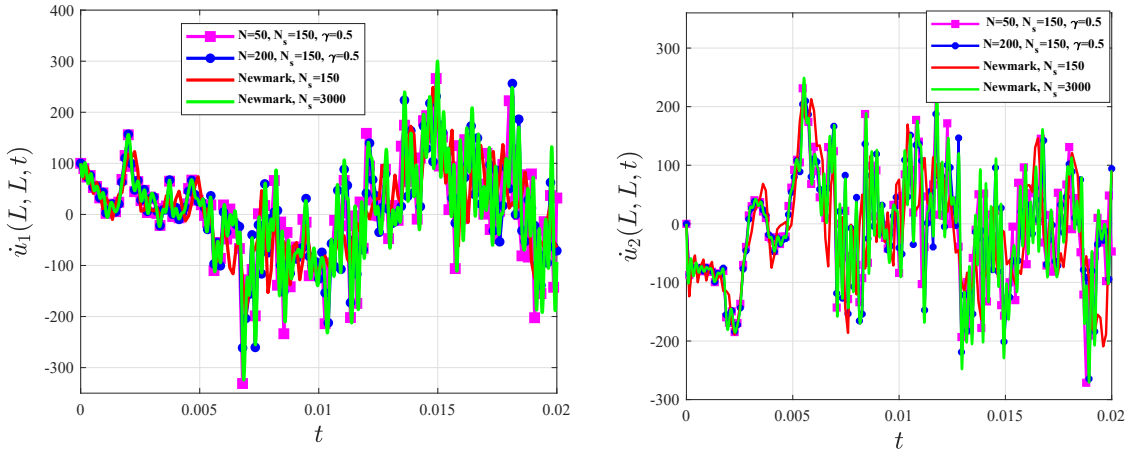

Figure 13: Horizontal and vertical velocity fields of the reference point for Saint Venant-Kirchhoff material ($T^{total} = 0.02s$).

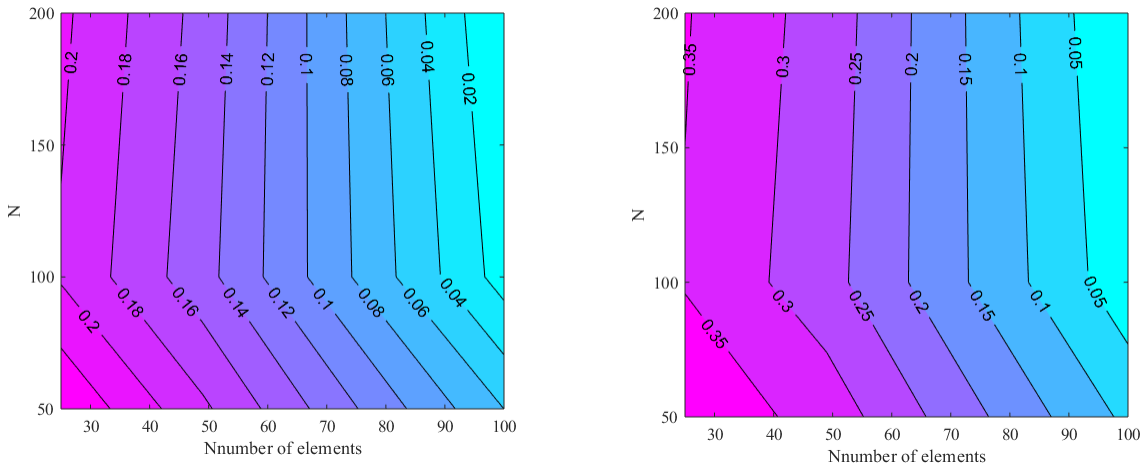

(a) Horizontal displacement.

(b) Vertical displacement.

Figure 14: The error-index (6.7) in terms of number of elements and time-wise terms for the Saint Venant-Kirchhoff plate ($N_s = 150$ and $\gamma = 0.5$).

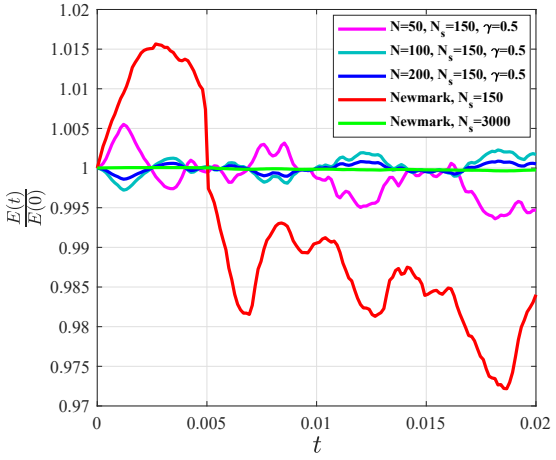

Figure 15: The energy function for the free vibration of the Saint Venant-Kirchhoff plate material ($T^{total} = 0.02s$).

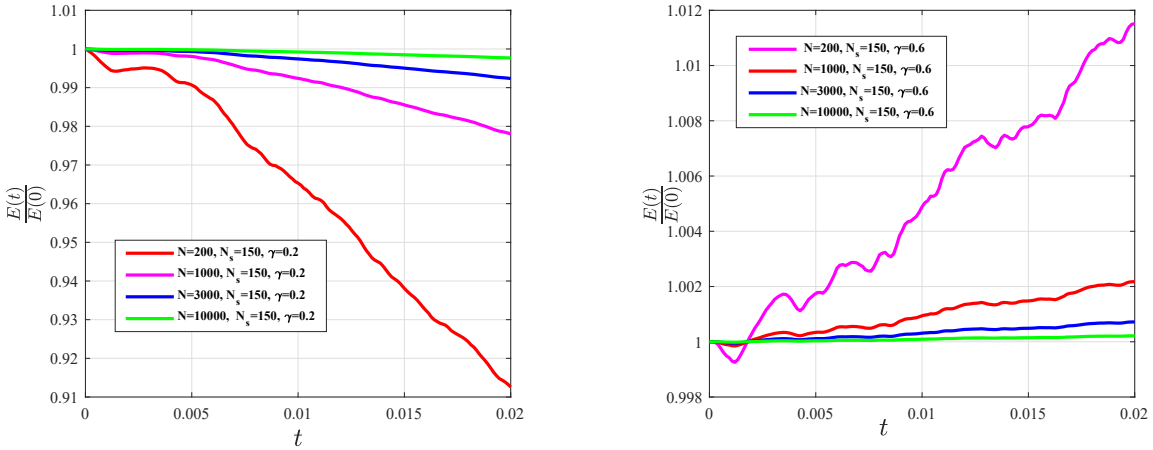

(a) $\gamma = 0.2$. (b) $\gamma = 0.6$.

Figure 16: The effect of γ on conservation of energy for the Saint Venant-Kirchhoff plate.

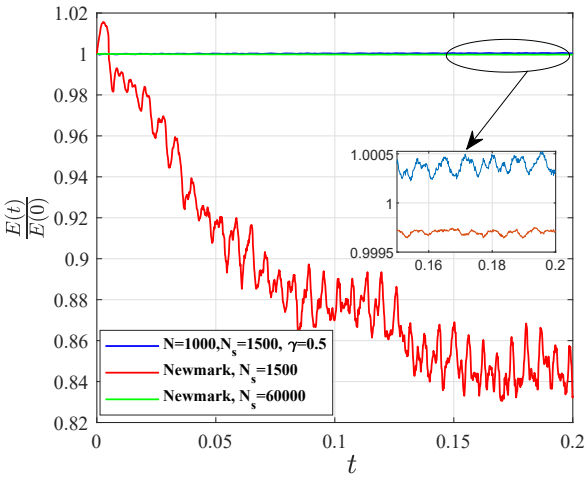

Figure 17: Conservation of the energy for a relatively longer time interval for Saint Venant-Kirchhoff plate.

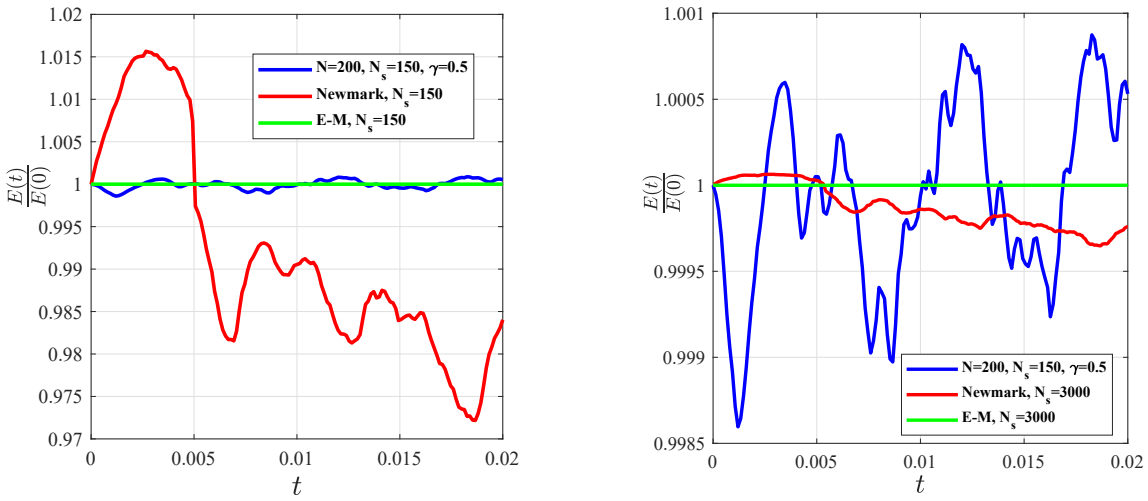

Figure 18: Comparison of energy between present study, Newmark average acceleration method, and the Energy-momentum algorithm, $T^{total} = 0.02s$.

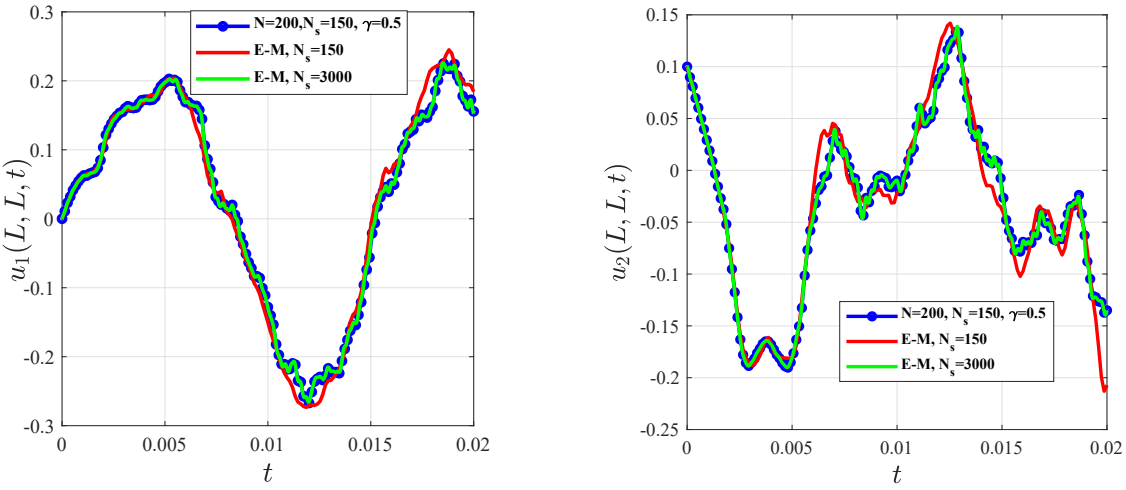

Figure 19: Comparison of displacement between present study and the Energy-momentum algorithm, $T^{total} = 0.02s$.

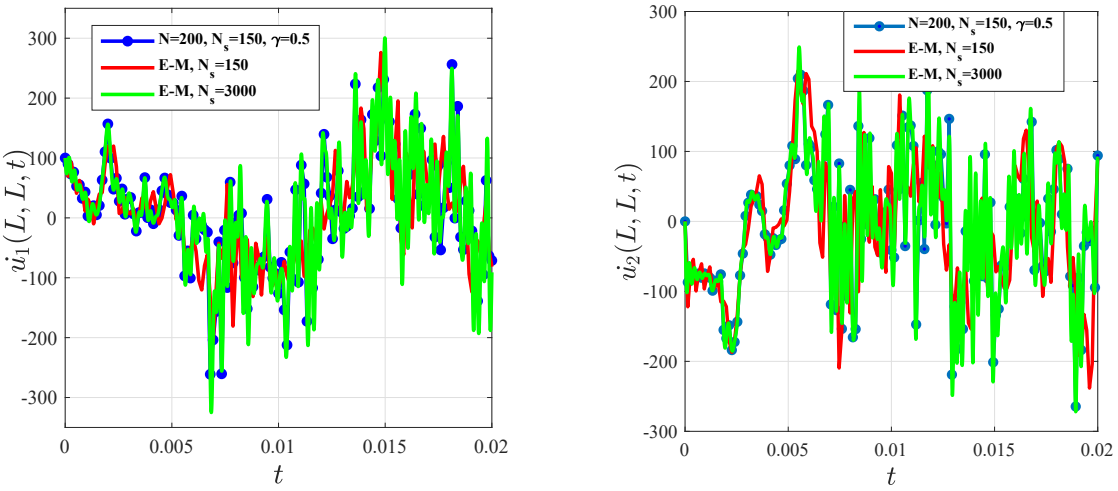

Figure 20: Comparison of velocity between present study and the Energy-momentum algorithm, $T^{total} = 0.02s$.

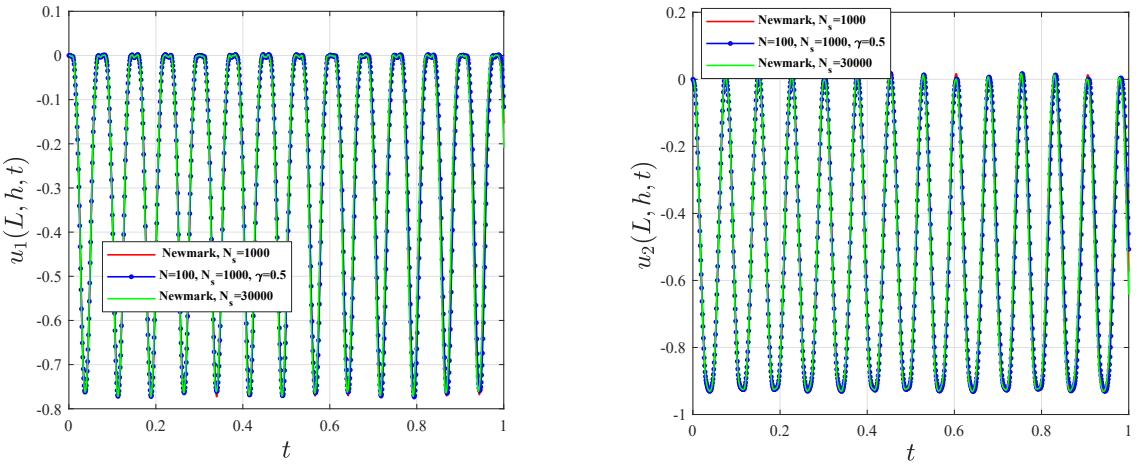

Figure 21: Horizontal and vertical displacements of the reference point for the nonlinear beam ($T^{total} = 1s$).

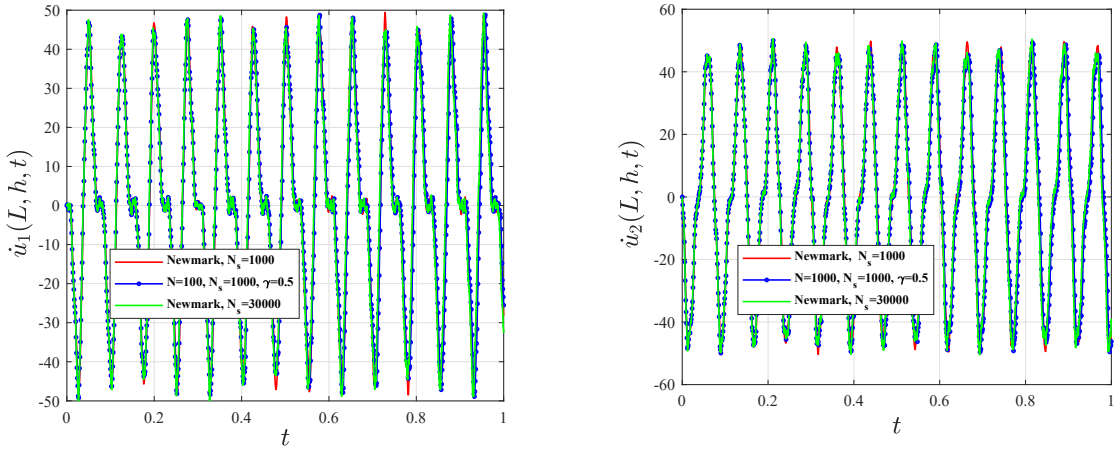

Figure 22: Horizontal and vertical velocities of the reference point for the nonlinear beam ($T^{total} = 1s$).

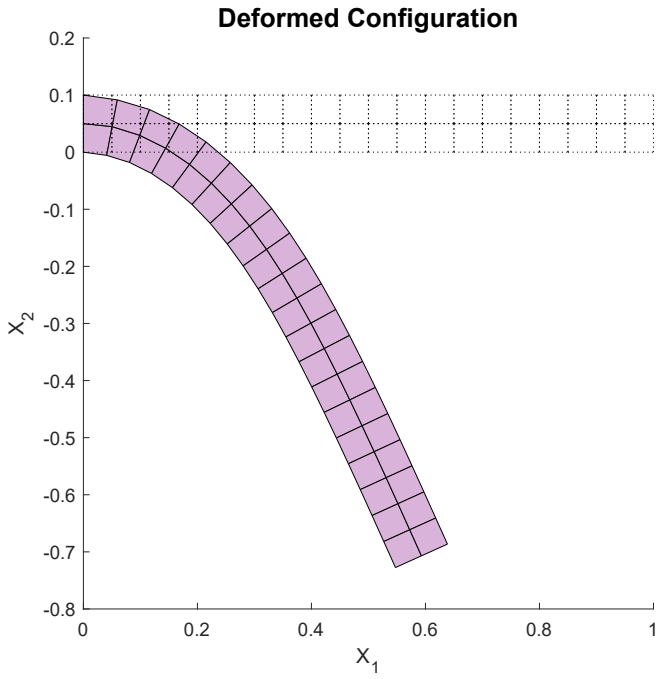

Figure 23: The deformed configuration at $t = 0.1s$ for the nonlinear beam.

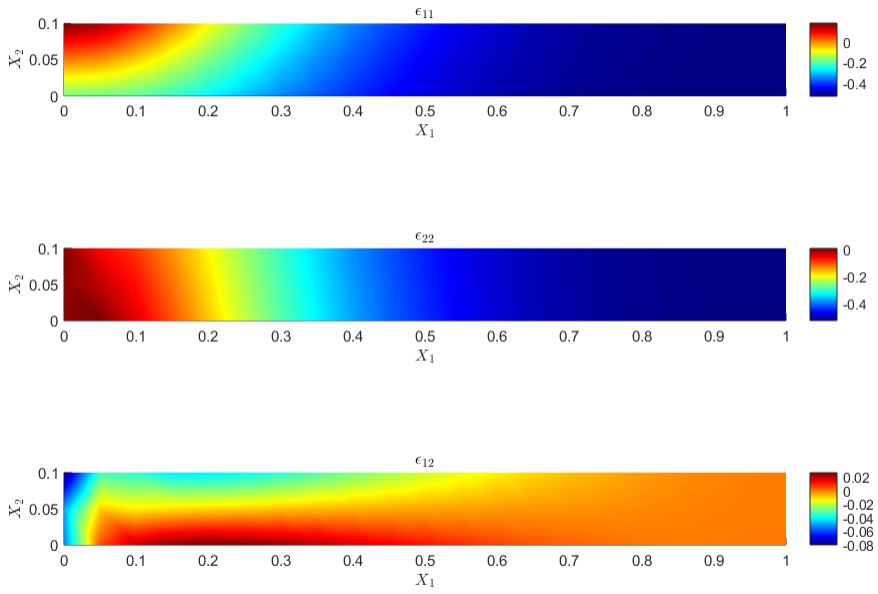

Figure 24: Infinitesimal strain field at $t = 0.1s$ for the nonlinear beam.

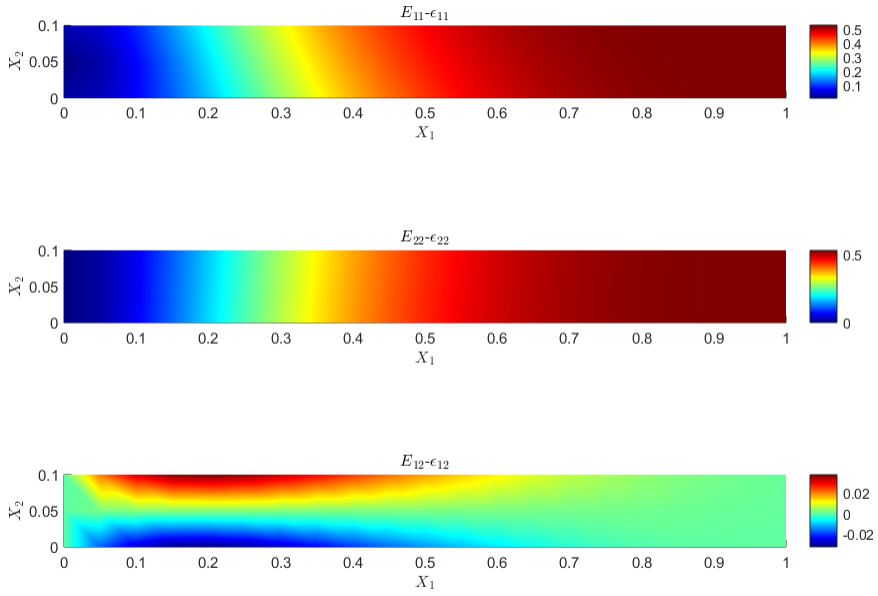

Figure 25: The difference between Green-Lagrange and infinitesimal strain fields at $t = 0.1s$ for the nonlinear beam.

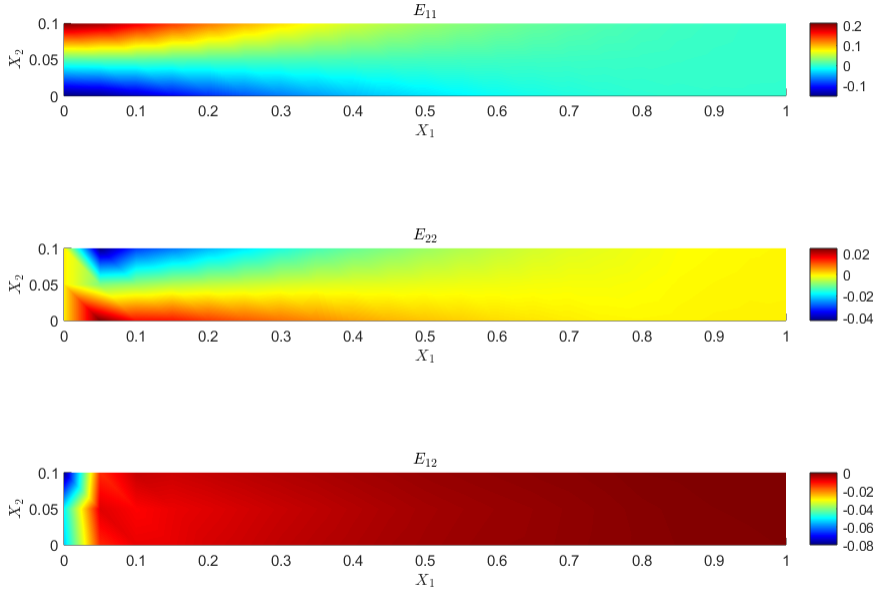

Figure 26: Green-Lagrange strain field at $t = 0.1s$ for the nonlinear beam.

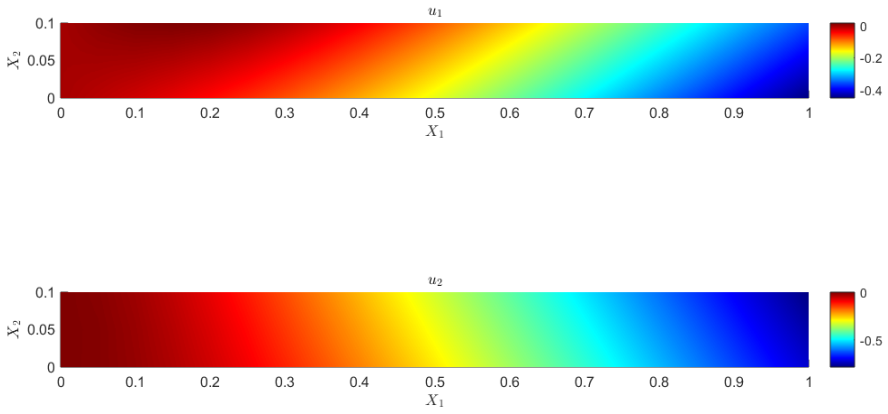

Figure 27: Displacement fields at $t = 0.1s$ for the nonlinear beam.

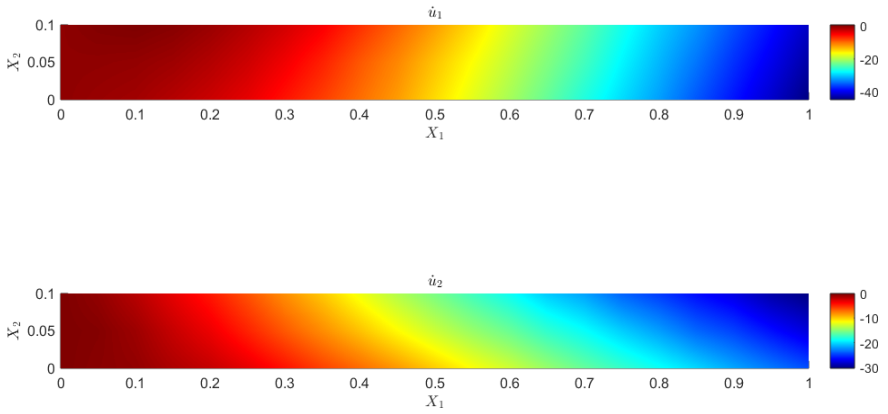

Figure 28: Velocity fields at $t = 0.1s$ for the nonlinear beam.

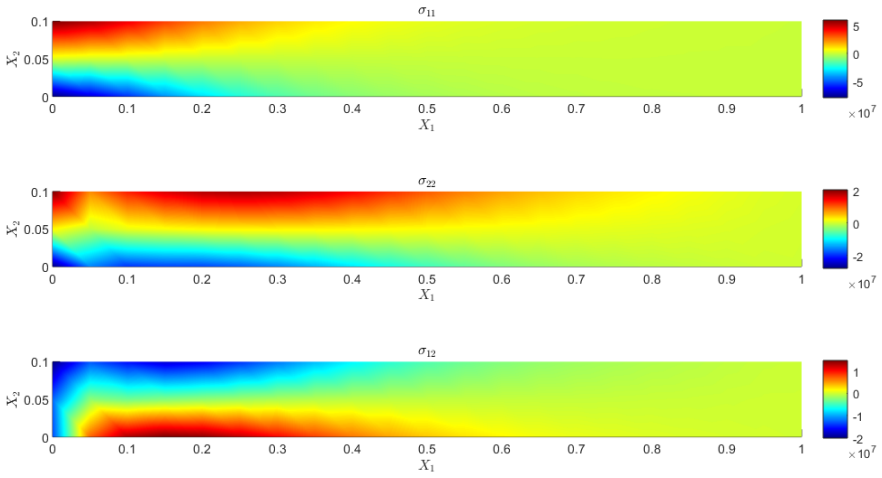

Figure 29: Stress components at $t = 0.1s$ for the nonlinear beam.

References

[1] T. J. R. Hughes, "Stability, convergence and growth and decay of energy of the average acceleration method in nonlinear structural dynamics," *Computers & Structures*, vol. 6, no. 4-5, pp. 313–324, 1976.

[2] D. Kuhl and M. Crisfield, "Energy-conserving and decaying algorithms in non-linear structural dynamics," *International Journal for Numerical Methods in Engineering*, vol. 45, no. 5, pp. 569–599, 1999.

[3] T. Hughes, T. Caughey, and W. Liu, "Finite-element methods for nonlinear elastodynamics which conserve energy," *Journal of Applied Mechanics*, vol. 45, no. 2, pp. 366–370, 1978.

[4] D. Kuhl and E. Ramm, "Constraint energy momentum algorithm and its application to non-linear dynamics of shells," *Computer Methods in Applied Mechanics and Engineering*, vol. 136, no. 3-4, pp. 293–315, 1996.

[5] J. E. Marsden and M. West, "Discrete mechanics and variational integrators," *Acta Numerica*, vol. 10, no. 1, pp. 357–514, 2001.

[6] G. Zhong and J. E. Marsden, "Lie-poisson Hamilton-Jacobi theory and Lie-Poisson integrators," *Physics Letters A*, vol. 133, no. 3, pp. 134–139, 1988.

[7] J. Simo and N. Tarnow, "The discrete energy-momentum method. Conserving algorithms for nonlinear elastodynamics," *ZAMP*, vol. 43, no. 5, pp. 757–792, 1992.

[8] O. Gonzalez, "Exact energy and momentum conserving algorithms for general models in nonlinear elasticity," *Computer Methods in Applied Mechanics and Engineering*, vol. 190, no. 13-14, pp. 1763–1783, 2000.

[9] T. Laursen and X. Meng, "A new solution procedure for application of energy-conserving algorithms to general constitutive models in nonlinear elastodynamics," *Computer Methods in Applied Mechanics and Engineering*, vol. 190, no. 46-47, pp. 6309–6322, 2001.

[10] F. Armero and I. Romero, "On the formulation of high-frequency dissipative time-stepping algorithms for nonlinear dynamics. part i: low-order methods for two model problems and nonlinear elastodynamics," *Computer Methods in Applied Mechanics and Engineering*, vol. 190, no. 20-21, pp. 2603–2649, 2001.

[11] F. Armero and I. Romero, "On the formulation of high-frequency dissipative time-stepping algorithms for nonlinear dynamics. part ii: second-order methods," *Computer Methods in Applied Mechanics and Engineering*, vol. 190, no. 51-52, pp. 6783–6824, 2001.

[12] R. A. LaBudde and D. Greenspan, "Energy and momentum conserving methods of arbitrary order for the numerical integration of equations of motion," *Numerische Mathematik*, vol. 25, no. 4, pp. 323–346, 1975.

[13] R. A. LaBudde and D. Greenspan, "Energy and momentum conserving methods of arbitrary order for the numerical integration of equations of motion," *Numerische Mathematik*, vol. 26, no. 1, pp. 1–16, 1976.

[14] I. Romero, "An analysis of the stress formula for energy-momentum methods in nonlinear elastodynamics," *Computational Mechanics*, vol. 50, no. 5, pp. 603–610, 2012.

[15] K.-J. Bathe, "Conserving energy and momentum in nonlinear dynamics: a simple implicit time integration scheme," *Computers & structures*, vol. 85, no. 7-8, pp. 437–445, 2007.

[16] P. Betsch and P. Steinmann, "Conservation properties of a time FE method—part ii: Time-stepping schemes for non-linear elastodynamics," *International Journal for Numerical Methods in Engineering*, vol. 50, no. 8, pp. 1931–1955, 2001.

[17] M. Groß, P. Betsch, and P. Steinmann, "Conservation properties of a time FE method. part iv: Higher order energy and momentum conserving schemes," *International Journal for Numerical Methods in Engineering*, vol. 63, no. 13, pp. 1849–1897, 2005.

[18] M. E. Gurtin, "Variational principles for linear elastodynamics," *Archive for Rational Mechanics and Analysis*, vol. 16, no. 1, pp. 34–50, 1964.

[19] A. Amiri-Hezaveh, A. Masud, and M. Ostoja-Starzewski, "Convolution finite element method: an alternative approach for time integration and time-marching algorithms," *Computational Mechanics*, pp. 1–30, 2021.

[20] R. E. Nickell and J. L. Sackman, "Variational principles for linear coupled thermoelasticity," *Quart. Appl. Math.*, vol. 26, no. 1, pp. 11–26, 1968.

[21] A. Amiri-Hezaveh, P. Karimi, and M. Ostoja-Starzewski, "Stress field formulation of linear electro-magneto-elastic materials," *Mathematics and Mechanics of Solids*, vol. 24, no. 12, pp. 3806–3822, 2019.

[22] A. Amiri-Hezaveh, P. Karimi, and M. Ostoja-Starzewski, "Ibvp for electromagneto-elastic materials: variational approach," *Mathematics and Mechanics of Complex Systems*, vol. 8, no. 1, pp. 47–67, 2020.

[23] A. Amiri-Hezaveh, H. Moghaddasi, and M. Ostoja-Starzewski, "Convolution finite element method for analysis of piezoelectric materials," To appear in *Computer Methods in Applied Mechanics and Engineering*.

[24] A. Amiri-Hezaveh and M. Ostoja-Starzewski, "A convolutional-iterative solver for nonlinear dynamical systems," *Applied Mathematics Letters*, vol. 130, p. 107990, 2022.

[25] O. Gonzalez and A. M. Stuart, *A First Course in Continuum Mechanics*, vol. 42. Cambridge University Press, 2008.

[26] P. Wriggers, *Nonlinear Finite Element Methods*. Springer Science & Business Media, 2008.

[27] N. S. Bakhvalov and L. Vasil'eva, "Evaluation of the integrals of oscillating functions by interpolation at nodes of gaussian quadratures," *USSR Computational Mathematics and Mathematical Physics*, vol. 8, no. 1, pp. 241–249, 1968.

[28] T. Patterson, "On high precision methods for the evaluation of fourier integrals with finite and infinite limits," *Numerische Mathematik*, vol. 27, no. 1, pp. 41–52, 1976.